NAVAL POSTGRADUATE SCHOOL

MONTEREY, CALIFORNIA

THESIS

TIME SERIES ANALYSIS OF VEGETATION CHANGE USING HYPERSPECTRAL AND MULTISPECTRAL DATA

by

Spencer A. Wahrman

September 2012

Thesis Advisor:	Fred A. Kruse
Second Reader:	Dar A. Roberts

Approved for public release; distribution is unlimited

THIS PAGE INTENTIONALLY LEFT BLANK

REPORT DOCUMENTATION PAGE			Form Approved OMB No. 0704–0188
Public reporting burden for this collection of information is estimated to average 1 hour per response, including the time for reviewing instruction, searching existing data sources, gathering and maintaining the data needed, and completing and reviewing the collection of information. Send comments regarding this burden estimate or any other aspect of this collection of information, including suggestions for reducing this burden, to Washington headquarters Services, Directorate for Information Operations and Reports, 1215 Jefferson Davis Highway, Suite 1204, Arlington, VA 22202–4302, and to the Office of Management and Budget, Paperwork Reduction Project (0704–0188) Washington DC 20503.			
1. AGENCY USE ONLY *(Leave blank)*	**2. REPORT DATE** September 2012	**3. REPORT TYPE AND DATES COVERED** Master's Thesis	
4. TITLE AND SUBTITLE Time Series Analysis of Vegetation Change using Hyperspectral and Multispectral Data		**5. FUNDING NUMBERS**	
6. AUTHOR(S) Spencer A. Wahrman			
7. PERFORMING ORGANIZATION NAME(S) AND ADDRESS(ES) Naval Postgraduate School Monterey, CA 93943–5000		**8. PERFORMING ORGANIZATION REPORT NUMBER**	
9. SPONSORING /MONITORING AGENCY NAME(S) AND ADDRESS(ES) N/A		**10. SPONSORING/MONITORING AGENCY REPORT NUMBER**	
11. SUPPLEMENTARY NOTES The views expressed in this thesis are those of the author and do not reflect the official policy or position of the Department of Defense or the U.S. Government. IRB Protocol number _____N/A_____.			
12a. DISTRIBUTION / AVAILABILITY STATEMENT Approved for public release; distribution is unlimited		**12b. DISTRIBUTION CODE** A	

13. ABSTRACT (maximum 200 words)

Grand Lake, Colorado has experienced a severe mountain pine beetle outbreak over the past twenty years. The aim of this study was to map lodgepole pine mortality and health decline due to mountain pine beetle. Multispectral data spanning a five-year period from 2006 to 2011 were used to assess the progression from live, green trees to dead, gray-brown trees. IKONOS data from 2011 were corrected to reflectance and validated against an Airborne Visible/Infrared Imaging Spectrometer (AVIRIS) hyperspectral dataset, also collected during 2011. These data were used along with additional reflectance-corrected multispectral datasets (IKONOS from 2007 and QuickBird from 2006 and 2009) to create vegetation classification maps using both library spectra and regions of interest. Two sets of classification maps were produced using Mixture-Tuned Matched Filtering. The results were assessed visually and mathematically. Through visual inspection of the classification maps, increasing lodgepole pine mortality over time was observed. The results were quantified using confusion matrices comparing the classification results of the AVIRIS classified data and the IKONOS and QuickBird classified data. The comparison showed that change could be seen over time, but due to the short time period of the data the change was not as significant as expected.

14. SUBJECT TERMS Type Keywords Here			**15. NUMBER OF PAGES** 97
			16. PRICE CODE
17. SECURITY CLASSIFICATION OF REPORT Unclassified	**18. SECURITY CLASSIFICATION OF THIS PAGE** Unclassified	**19. SECURITY CLASSIFICATION OF ABSTRACT** Unclassified	**20. LIMITATION OF ABSTRACT** UU

NSN 7540–01–280–5500 Standard Form 298 (Rev. 2–89)
Prescribed by ANSI Std. 239–18

THIS PAGE INTENTIONALLY LEFT BLANK

Approved for public release; distribution is unlimited

TIME SERIES ANALYSIS OF VEGETATION CHANGE USING HYPERSPECTRAL AND MULTISPECTRAL DATA

Spencer A. Wahrman
Civilian, Department of the Navy
B.A., University of Northern Colorado, 2006

Submitted in partial fulfillment of the
requirements for the degree of

MASTER OF SCIENCE IN REMOTE SENSING INTELLIGENCE

from the

NAVAL POSTGRADUATE SCHOOL
September 2012

Author: Spencer A. Wahrman

Approved by: Fred A. Kruse
Thesis Advisor

Dar A. Roberts
Second Reader

Dan Boger
Chair, Department of Information Sciences

THIS PAGE INTENTIONALLY LEFT BLANK

ABSTRACT

Grand Lake, Colorado has experienced a severe mountain pine beetle outbreak over the past twenty years. The aim of this study was to map lodgepole pine mortality and health decline due to mountain pine beetle. Multispectral data spanning a five-year period from 2006 to 2011 were used to assess the progression from live, green trees to dead, gray-brown trees. IKONOS data from 2011 were corrected to reflectance and validated against an Airborne Visible/Infrared Imaging Spectrometer (AVIRIS) hyperspectral dataset, also collected during 2011. These data were used along with additional reflectance-corrected multispectral datasets (IKONOS from 2007 and QuickBird from 2006 and 2009) to create vegetation classification maps using both library spectra and regions of interest. Two sets of classification maps were produced using Mixture-Tuned Matched Filtering. The results were assessed visually and mathematically. Through visual inspection of the classification maps, increasing lodgepole pine mortality over time was observed. The results were quantified using confusion matrices comparing the classification results of the AVIRIS classified data and the IKONOS and QuickBird classified data. The comparison showed that change could be seen over time, but due to the short time period of the data the change was not as significant as expected.

THIS PAGE INTENTIONALLY LEFT BLANK

TABLE OF CONTENTS

LIST OF FIGURES

LIST OF TABLES

THIS PAGE INTENTIONALLY LEFT BLANK

LIST OF ACRONYMS AND ABBREVIATIONS

AFB	Air Force Base
AVIRIS	Airborne Visible/InfraRed Imaging Spectrometer
ETM+	Enhanced Thematic Mapper Plus
FLAASH	Fast Line of Sight Atmospheric Analysis of Spectral Hypercubes
GCP	Ground Control Point
HSI	Hyperspectral Imaging
km	Kilometer
MF	Matched Filter
µm	Micrometer
MNF	Minimum Noise Fraction
MSI	Multispectral Imagery
MSS	Multispectral Scanner System
MTMF	Mixture-Tuned Matched Filtering
NDVI	Normalized Difference Vegetation Index
nm	Nanometer
PCA	Principal Components Analysis
RGI	Red-Green Index
ROI	Region of Interest
SNR	Signal to Noise Ratio
SWIR	Shortwave InfraRed
TCT	Tasseled Cap Transformation
VNIR	Visible and Near InfraRed

THIS PAGE INTENTIONALLY LEFT BLANK

ACKNOWLEDGMENTS

I would like to thank the numerous people and one animal that helped me to complete this study. I would like to thank my dog, Angus. Through the thesis writing process he has suffered with me, not getting nearly the amount of exercise or caring he deserves. I would also like to thank Dr. Fred Kruse for keeping me motivated and dedicated to writing a thesis that would not only satisfy him, but would make me proud. This was not the easiest road to travel, but he steered me onward with wonderful guidance and support. Finally, to the wonderful friends I have made while at the Naval Postgraduate School. Thank you for the hours of support and laughter you have all provided. To Steve Terry for never saying no to a night out. To Willy Hall for listening to my incessant yammering day in and day out. To Jason Suckstorff for never getting angry with me, even though I may have deserved it. To Corey Bangs for his dry wit and always providing a good joke. To Christina Mayberry for letting me vent my frustrations over and over and over again. To Mallory DeCoster for being a wonderful friend all the time, even when I may not have deserved her friendship. And to Krista Lee, without whom I would not have come to know the Naval Postgraduate School or any of the amazing people I have met while living in Monterey, California.

THIS PAGE INTENTIONALLY LEFT BLANK

I. INTRODUCTION

Mountain pine beetles (*Dendroctonus ponderosae*) and other infestation and stress situations have killed a considerable amount of forest on the North American continent over the last twenty years (Wulder et al., 2006). The changes effected by the mountain pine beetle present a number of questions related to forest ecosystems, economies and the environment. Benefits that forests provide, besides the obvious aesthetic pleasure, include; wood products, recreational opportunities, water shed control, carbon storage, temperature moderation, fostering habitats, and mitigating fire danger. In Colorado, forests and woodlands cover 9.87 million hectares of land surface, of which conifer forests are the most predominant (Colorado State Forest Service, 2011). Mountain pine beetle (MPB) outbreaks are cyclical, occurring over periods of warm, dry weather (White et al., 2005). There are natural predators of pine beetles, including woodpeckers and other insects, however, extreme cold temperatures resulting in a severe freeze are required to effectively kill off MPB (Leatherman et al., 2011). Since the current outbreak of mountain pine beetles erupted over twenty years ago in North America, forest landscapes across the continent have changed dramatically. In North America, specifically in Colorado, mountain pine beetles have been the most damaging forest pest. Since the first detection of infestation in 1996 (Associated Press, 2008), of 1.34 million hectares of Colorado's pine forests have been impacted (Colorado State Forest Service, 2011).

Mountain pine beetles typically attack, "trees that are not growing vigorously due to old age, crowding, poor growing conditions, drought, fire or mechanical damage" (Leatherman et al., 2011). Pine tree damage occurs coincidentally with the maturation of mountain pine beetles, usually over a one year period (Wulder et al., 2006). Trees affected by pine beetles go through a number of stages before they ultimately die: green healthy, green attacked, red/orange attack, and grey kill (Wulder et al., 2006). After only twelve months, 90 percent of killed trees will exhibit red needles. Three years after being attacked most trees will have shed all needles, considered grey kill.

Remote sensing data have been used to help track the changes of the forests, however; methods for detecting, mapping, tracking, and predicting degradation are not well developed or fully validated (DeRose et al., 2011; Meddens et al. 2011; Skakun et al., 2003; White et al., 2005; Wulder et al., 2006;). The goal of this study was to examine methods for detecting and monitoring spectral changes in vegetation using hyperspectral and multispectral data. This research used a time series of imagery of a specific problem area in Colorado to test mapping methods and to determine whether or not annual patterns exist. The research examined the feasibility and accuracy of using hyperspectral and multispectral data to find unique spectral signatures of coniferous trees at different stages of health, and to create a model showing past and current kill areas in Colorado's montane forests.

II. BACKGROUND

A. OVERVIEW OF MULTISPECTRAL AND HYPERSPECTRAL IMAGERY

1. Remote Sensing

Electro-optical remote sensing is the acquisition of imagery from an object without coming into physical contact with that object (Shaw & Burke, 2003). Data produced by aircraft or satellites can be used to observe a number of characteristics of the Earth's surface. Through these data, specific features can be detected, painting a very unique picture of what materials exist in an area of interest (Schowengerdt, 2007). Remote sensing systems provide a valuable resource in Earth observation. By allowing for repeated coverage over an area, both human and natural events can be observed. With the advances and developments in remote sensing technology Earth observation today is easier than ever before.

Today, aerial- and space-based remote sensors provide a significant resource for civil and military applications. With advances in camera and sensor technology, data provided by satellites and airborne vehicles have become much more sophisticated. Technology has improved immensely since the launch of the first Landsat Multispectral Scanner System (MSS) in 1972, which allowed acquisition of images at multiple wavelengths of the electromagnetic spectrum (Schowengerdt, 2007). Today, as with Landsat MSS before, these sensors require a natural source of electromagnetic radiation from the sun in order to produce imagery (Eismann, 2012). Known as passive remote sensing systems, these sensors measure the energy received after it has been reflected off the Earth's surface (Fantle, 2010); see Figure 1. Data provided from remote sensing systems come in a variety of forms and data types. Two common types of data provided by these sensors are multispectral and hyperspectral images (see definitions below).

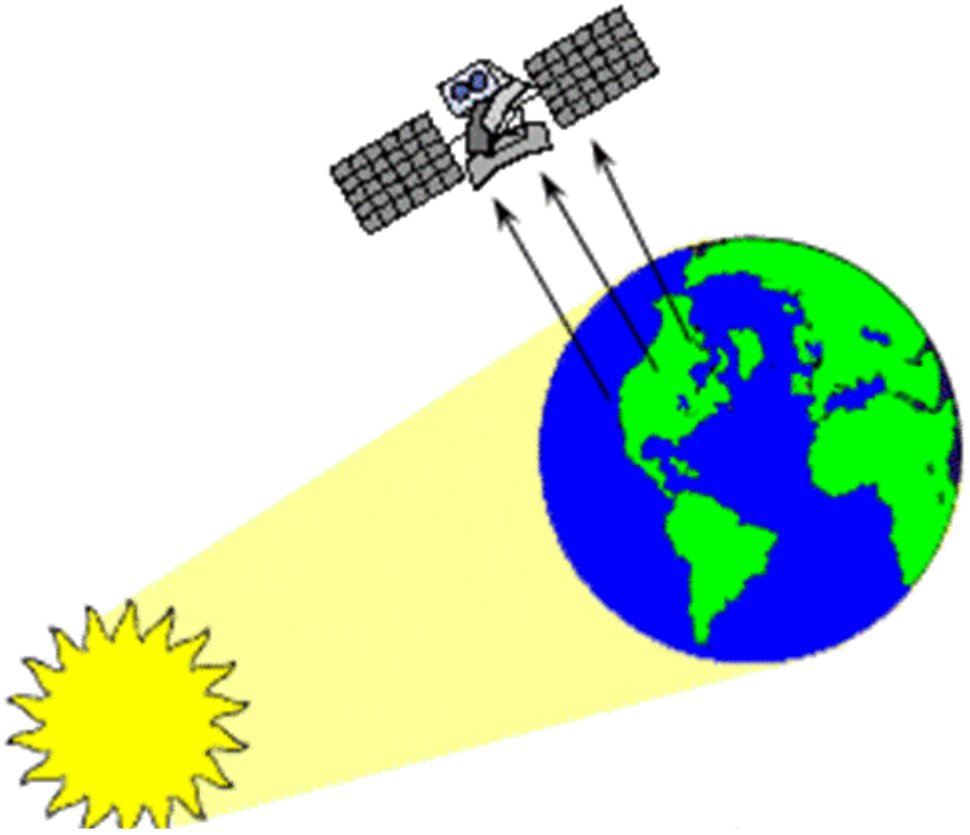

Figure 1. Illustration of passive remote sensing system (From Fantle, 2010).

2. Electromagnetic Spectrum

Remote sensing systems use selected regions of the electromagnetic spectrum to create images. The electromagnetic spectrum can be broken into five distinct parts, excluding Radar, Gamma, etc.: visible from 0.4–0.7 µm (the portion of the EM spectrum that human eyes can see (Mattson, 2010)), near infrared from 0.7–1.2 µm, shortwave infrared from 1.2–3.0 µm, midwave infrared from 3.0–5.0 µm, and long wave infrared from 5.0–14.0 µm (Eismann, 2012); see Figure 2. Each region of the spectrum has unique characteristics that capture different characteristics of the surface. By placing bands at certain wavelengths along the spectrum, different materials and features can be detected, and potentially identified. Passive remote sensing systems such as multispectral and hyperspectral sensors use the visible and near infrared (VNIR) through shortwave infrared (SWIR) regions of the EM spectrum

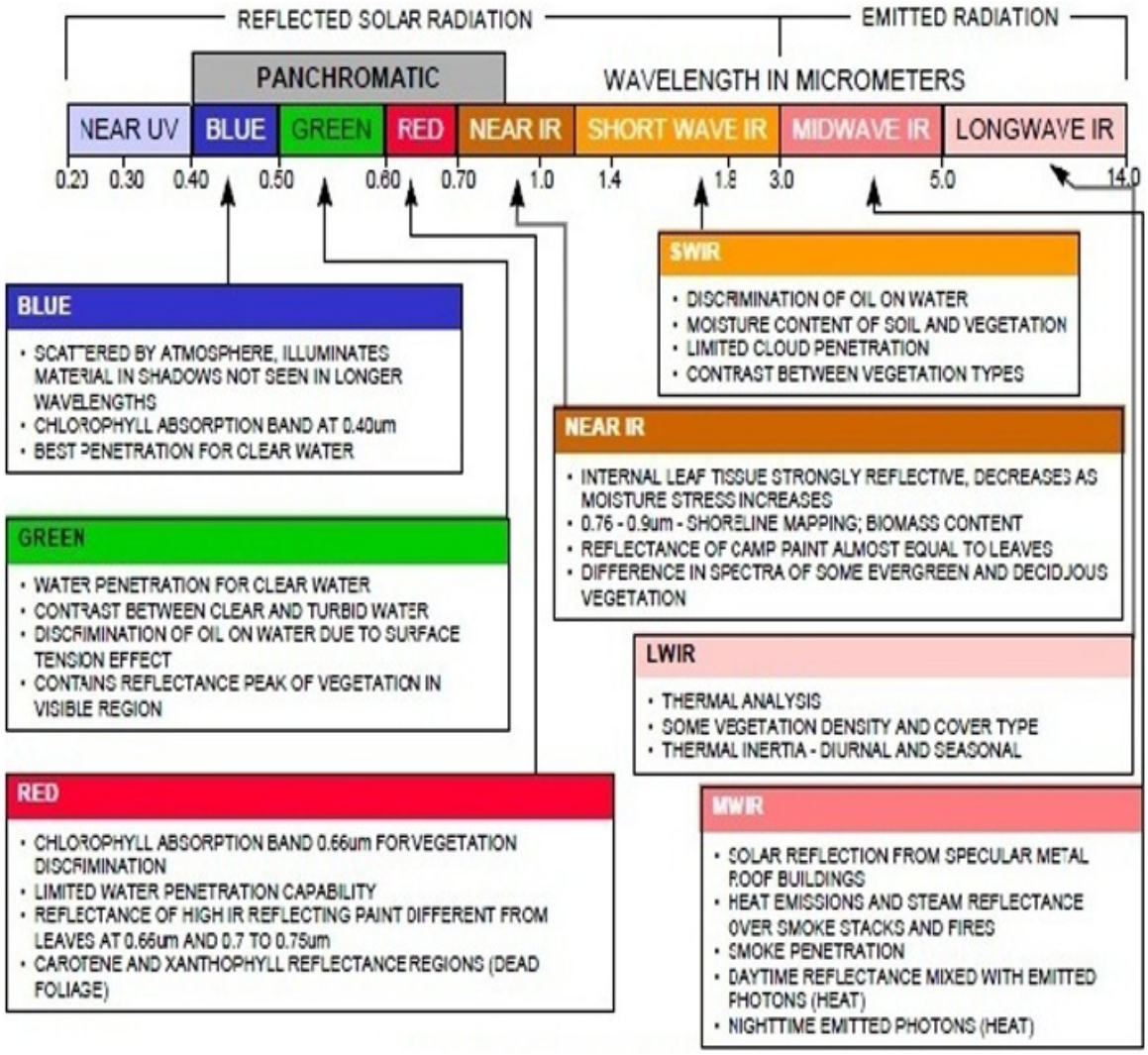

Figure 2. Electromagnetic spectrum (From AU Space Primer, 2002)

3. Multispectral Imaging

Spectral imaging refers to capturing an object at multiple wavelengths on the electromagnetic spectrum (Shaw & Burke, 2003). Combinations of bands are chosen at different spectral regions with the intent to detect spectral reflectance differences between materials of interest (Lillesand & Kiefer, 1994). A spectrum is the distribution of some measure of light power or material property with optical wavelength (Eismann, 2012). Based on how the material interacts with light, it is possible to detect the chemical

composition of the material (Eismann, 2012). Information about the surface composition is gathered by examining the intensity of the imagery in the selected bands (Eismann, 2012).

Once a scene is captured, a digital image is created with brightness values assigned to each pixel of the image. The images produced from each of the spectral bands are registered spatially by pixel to create an image that shows identical parts of the scene (Eismann, 2012); see Figure 3. In spectral imaging, sensors are spaced around the center of certain bands. Multispectral imaging typically uses the centers of the red (0.65µm), green (0.55µm), and blue (0.45µm) bands, but also makes use of the near infrared band at 0.7µm. The near infrared band is very useful in vegetation studies, allowing for easy distinction between healthy and unhealthy vegetation. Vegetation "typically has a low reflectance in the visible spectral region because of strong absorption by chlorophylls, a relatively high reflectance in the near-infrared because of internal leaf scattering and no absorption" (Knipling, 1970). By setting the center of each band at a specific wavelength, different spectral characteristics can be detected (Figure 3). Knowing those spectral characteristics makes classification and thematic mapping possible. This type of analysis enables the breakdown of regions by surface type based on spectral content, or object detection based on those spectra. In multispectral imaging this is limited, however, due to the lack of full spectral information based on the number of spectral bands used (usually about 3 to 10) (Eismann, 2012).

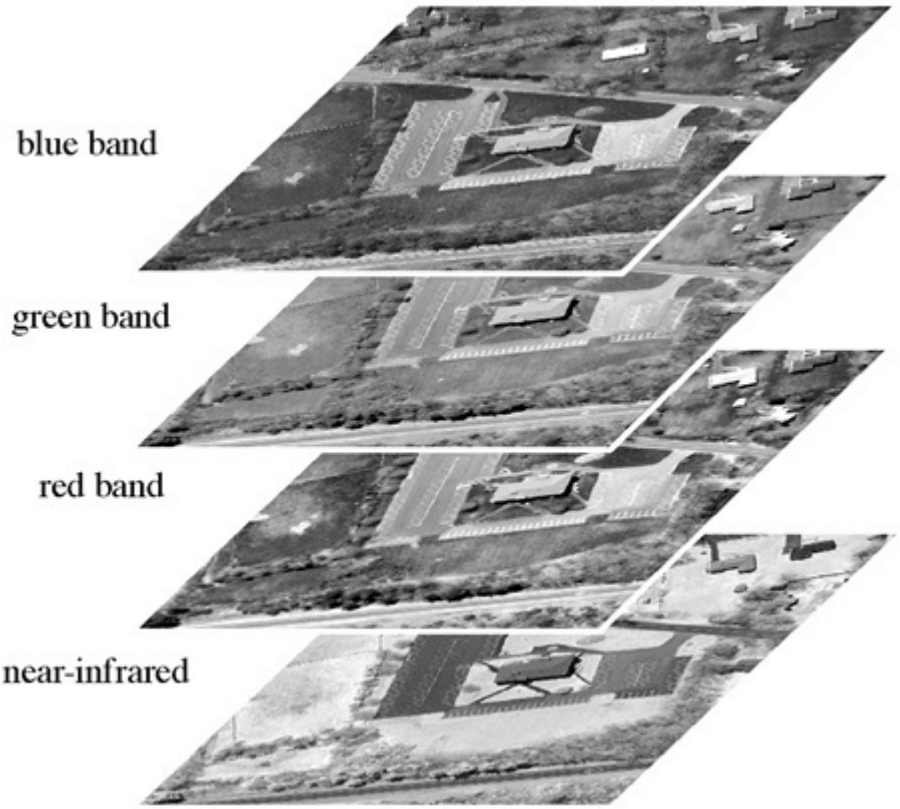

Figure 3. Multispectral image cube (From Jensen, 2005)

4. Hyperspectral Imaging

The use of multispectral image data for mapping materials and terrain is used frequently; however, due to the limited number of spectral bands, it is often difficult to accurately identify individual spectral features, and thus materials. Imaging spectrometry (hyperspectral imaging, HSI) developed from this need to fully characterize the signatures, to better understand the spectra collected from multispectral sensors, and to understand the causes of those signatures (Goetz, 2012). Defined as "the simultaneous acquisition of images in many narrow, contiguous spectral bands throughout the visible and solar reflected infrared portions of the spectrum," imaging spectrometry enables more in depth analysis of materials in a scene (Goetz et al., 1985). This is accomplished through the use of narrower sensor spectral channels. Instead of channels being spaced something like 100nm apart, imaging spectrometry typically uses band spectral resolution and critical band spacing of approximately 10 nm (Goetz et al., 1985). The narrow

spacing of the bands creates a finer spectrum, making individual features on each spectrum easier to identify (Figure 4). Hyperspectral imaging (HSI) uses the "same physical underpinning as the exploitation of multispectral imagery to extract scene information; in this case, however, the finer spectral sampling results in a greater wealth of information from which to ascertain the physical characteristics of the imaged objects" (Eismann, 2012).

Hyperspectral remote sensing has become a fairly well established method for mapping the Earth's surface. Hyperspectral imagery can be used in a number of fields and "its utility for ecological studies is virtually unlimited," with many applications: forestry management, agricultural studies, mineral exploration, environmental monitoring, and national security (Ustin et al., 2004; Blakenship, 2006).

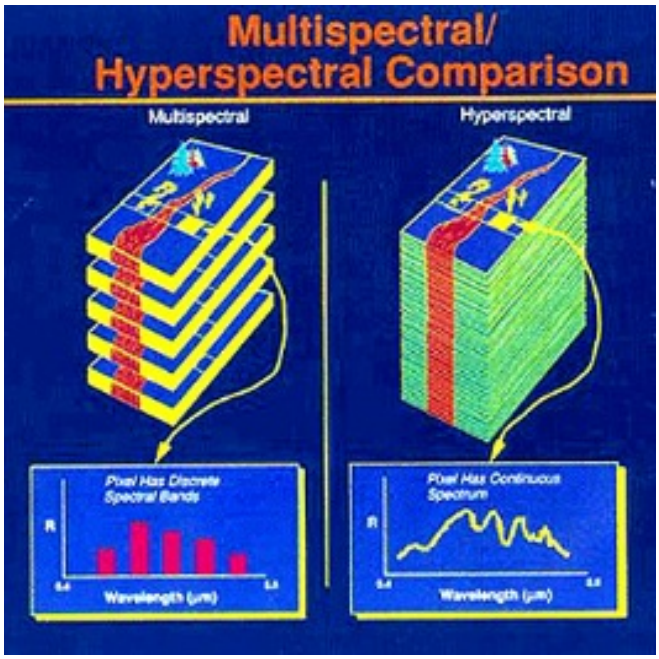

Figure 4. Comparison of multispectral image cube and hyperspectral image cube (From Short, 2007).

B. REMOTE SENSING SYSTEMS AND DATA

1. Systems

This study used multispectral commercial satellite imagery from DigitalGlobe's QuickBird and GeoEye's IKONOS satellites, and aerial imagery from NASA's AVIRIS hyperspectral imaging system.

a. IKONOS

IKONOS (Figure 5) is the first commercial remote sensing satellite to produce sub-meter imagery. Launched in 1999 from Vandenberg Air Force Base, IKONOS is in a polar, sun-synchronous orbit with an altitude of 681 km. The sensor offers panchromatic and multispectral images with spatial resolutions of 0.82 m and 3.2 m, respectively. IKONOS has five spectral bands: panchromatic, blue, green, red, and near infrared; with wavelengths spaced from 526 nm to 929 nm (0.526 µm to 0.920 µm) in the panchromatic bands, and 445 nm to 853 nm (0.445 µm to 0.853 µm) for the multispectral bands (GeoEye, 2012). It features a dynamic range of 11-bits per pixel, a swath width of 11.3 km, direct downlink to more than a dozen ground stations worldwide, and a revisit time of less than three days (GeoEye, 2012).

Figure 5. Artistic rendering of IKONOS satellite (From *Satnews Daily*, 2010).

b. QuickBird

The QuickBird satellite was the first satellite launched by DigitalGlobe (DigitalGlobe, 2012) (Figure 6). Launched in 2001 from Vandenberg Air Force Base, QuickBird is in a polar, sun-synchronous orbit at an altitude of 482 km, with an expected gradual descent to 450 km (DigitalGlobe, 2012). At the time of launch QuickBird had the highest spatial resolution of any commercial remote sensing satellite with 0.65 m panchromatic spatial resolution and 2.62 m multispectral spatial resolution. The sensor has five spectral bands panchromatic, blue, green, red, and near infrared; with wavelengths spaced from 405 nm to 1053 nm (0.405 µm to 1.053 µm) in the panchromatic band, and 430 nm to 918 nm (0.430 µm to 0.918 µm) for the multispectral bands. QuickBird features a dynamic range of 11-bits per pixel, 128 Gb of onboard storage capacity, a swath width of 18 km at 482 km altitude and 16.8 km at 450 km altitude, and a revisit time of 2.5 days (DigitalGlobe, 2012).

Figure 6. Artistic rendering of QuickBird (From DigitalGlobe, 2012).

c. AVIRIS

AVIRIS stands for “Airborne Visible/InfraRed Imaging Spectrometer” (Figure 7). This is a hyperspectral sensor, having 224 contiguous spectral bands with wavelengths from 380 nm to 2500 nm (0.38 µm to 2.5 µm). The sensor has been operated on four different aircraft platforms, NASA’s ER-2 jet, Twin Otter International’s turboprop, Scaled Composites’ Proteus, and NASA’s WB-57 (Jet Propulsion Laboratory 2012). AVIRIS is flown at altitudes of 4 km to 20 km above sea level, with spatial resolutions ranging accordingly from 4 m to20 m. In addition at 4 km altitude the swath width is 2 km, while at 20 km altitude the swath width is 11 km (Jet Propulsion Laboratory 2012). AVIRIS uses three detectors, silicon (Si) for visible wavelengths, indium gallium arsenide (InGaAr) for near infrared wavelengths, and indium antimonide (InSb) for shortwave infrared wavelengths (Jet Propulsion Laboratory 2012). Processed AVIRIS data are approximately 140 Megabytes for every 512 scanlines of data, called a scene. Each scene corresponds to an area of about 10 km in length on the ground (Green et al., 1998; Jet Propulsion Laboratory 2012).

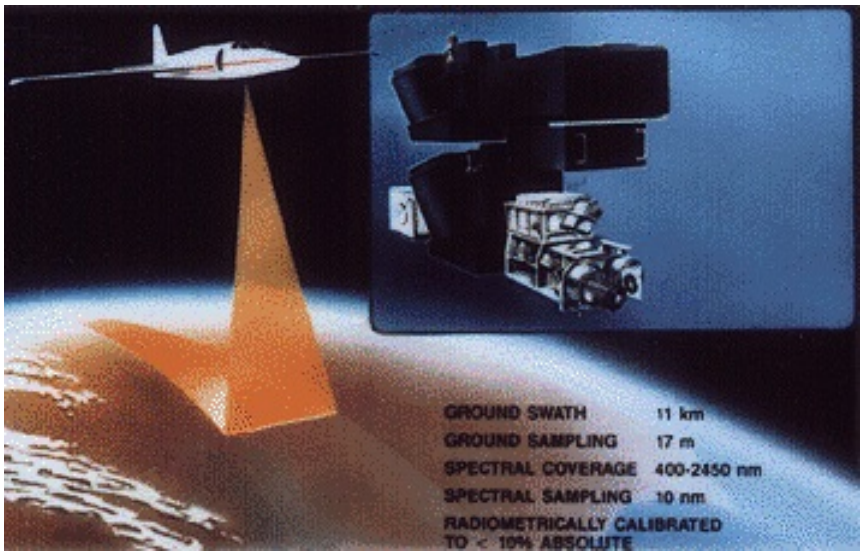

Figure 7. Artistic rendering of an AVIRIS flight onboard an ER-2 aircraft. The inset is a photo of the AVIRIS sensor (From Jet Propulsion Laboratory 2012).

2. Data

Two IKONOS and two QuickBird scenes were used for this research, and one AVIRIS image was used for this analysis. The IKONOS scenes have 4-meter spatial resolution, while the QuickBird images have 2.4-meter spatial resolution; the AVIRIS scene has a spatial resolution of 8.9 meters. The dates of the scenes range from 2006 to 2011. All of the scenes were acquired during summer months, from June to September (Table 1).

	Sensor	Scene ID	Resolution
2006 (Sept)	QuickBird	06SEP04181407	2.4m
2007 (Aug)	IKONOS	po_908079_0000000	3.7m
2009 (July)	QuickBird	09JUL07175737	2.4m
2011 (June)	IKONOS	po_908081_0000001	3.7m
2011 (Aug)	AVIRIS	f110807t01p00r06rdn	8.9m

Table 1. Collection sensor and date, and resolution of data used.

C. OVERVIEW OF STUDY AREA AND PREVIOUS WORK

1. Arapaho National Forest

Arapaho National Forest is located in north central Colorado along the western edge of Rocky Mountain National Park, and the Continental Divide. The forest is home to varying species of trees, but is largely populated by lodgepole pine (*Pinus contorta*) (Bobbe et al., 1994). Comprising 292,889 hectares, the landscape is dominated by the Rocky Mountains, parts of the Colorado River and South Plate River, and multiple reservoirs (United States Forest Service, 2007). Lodgepole pine grows in abundance in this area, preferring the high altitudes and moderate temperatures that are provided. For approximately the past thirty years the trees have been under attack by mountain pine beetle, having been largely decimated from sustained attacks by the insect (Hartman,

2008). This is especially evident in the area around Lake Granby in Grand County Colorado, where it is barely evident that mature lodgepole pine once inhabited the area.

When major logging operations ceased in the area over eighty years ago, lodgepole pines were allowed to grow unencumbered; additionally major fire suppression in the area has aided in the ascendance of these trees (Colorado State Forest Service 2006). This made the (monoculture) trees that populated the area decades later perfect hosts for mountain pine beetle (Madrigal, 2007). The impact has been severe, creating economic, environmental and recreational issues throughout the area. As the trees dry out and eventually die, fuel for forest fires is in abundant supply (Jenkins et al., 2012). Water supplies are in danger also, as a lack of soil cover "could leave reservoirs and rivers clogged with sediment" (Hartman, 2008). In addition, backpackers, campers, and skiers are in danger of being hit by falling trees. Mountain economies are hurt as well, as the brown backdrop is a less than appealing sight.

The area of interest for this study was the area on the north side of Lake Granby known as Green Ridge (Figure 8). This site has been dramatically affected by mountain pine beetle, which optimized the probability of obtaining useful remote sensing results.

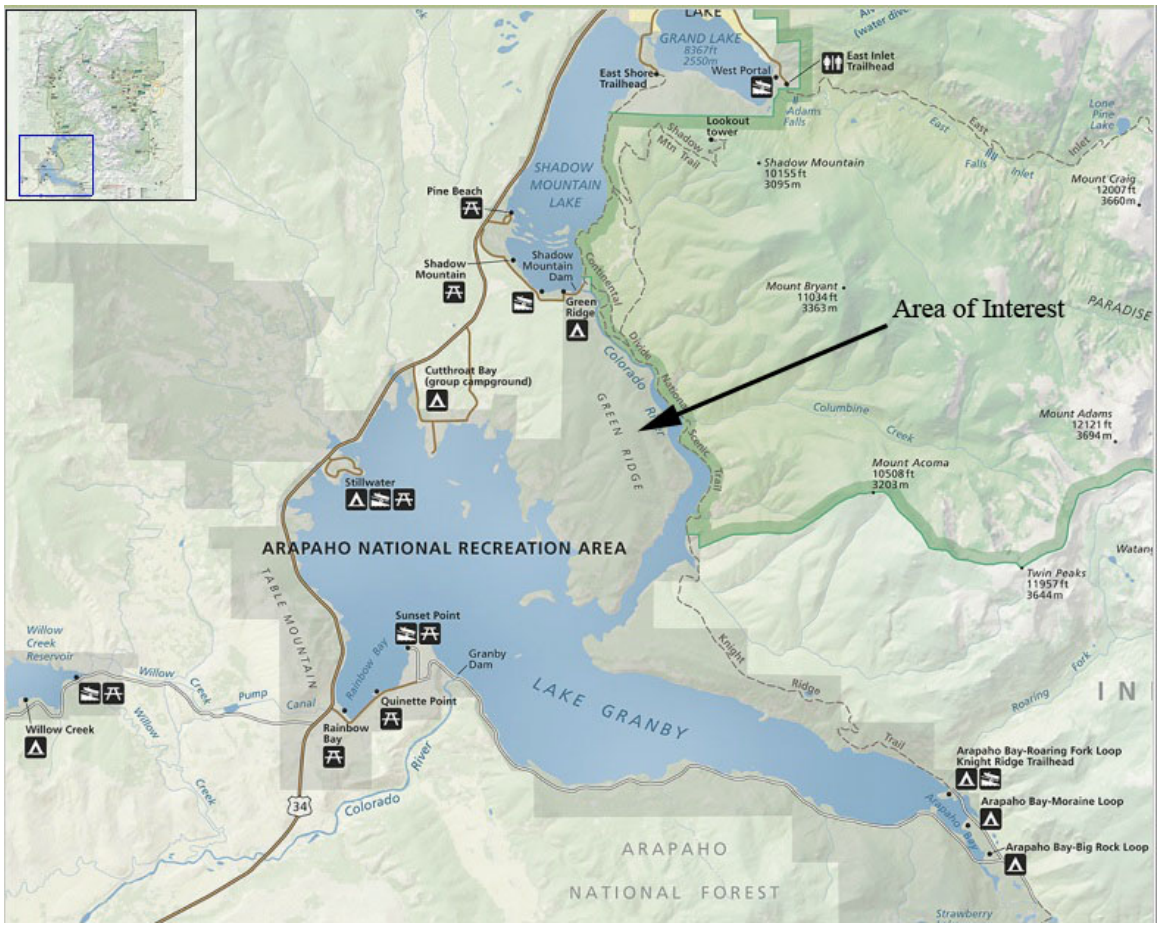

Figure 8. Lake Granby and Arapaho National Forest Area (From National Park Service)

2. Mountain Pine Beetle

Mountain pine beetle move through mature tree stands, killing those trees that have stopped growing "due to old age," trees that are overcrowded, those living in poor growing conditions, or have been affected by drought, fire or mechanical damage, or have root disease (Leatherman, 2011). These insects have changed forest landscapes across western North America over the past twenty years (Romme et al., 1986); see Figure 9. Killing thousands of hectares of pine trees from British Columbia to northern Mexico, mountain pine beetles are an extremely menacing pest (Wulder et al., 2006). Pine beetle kill is most severe during long periods of warm, dry weather. Since 2002, a period when temperatures have been favorable across North America, pine beetle populations have risen dramatically (White et al., 2005).

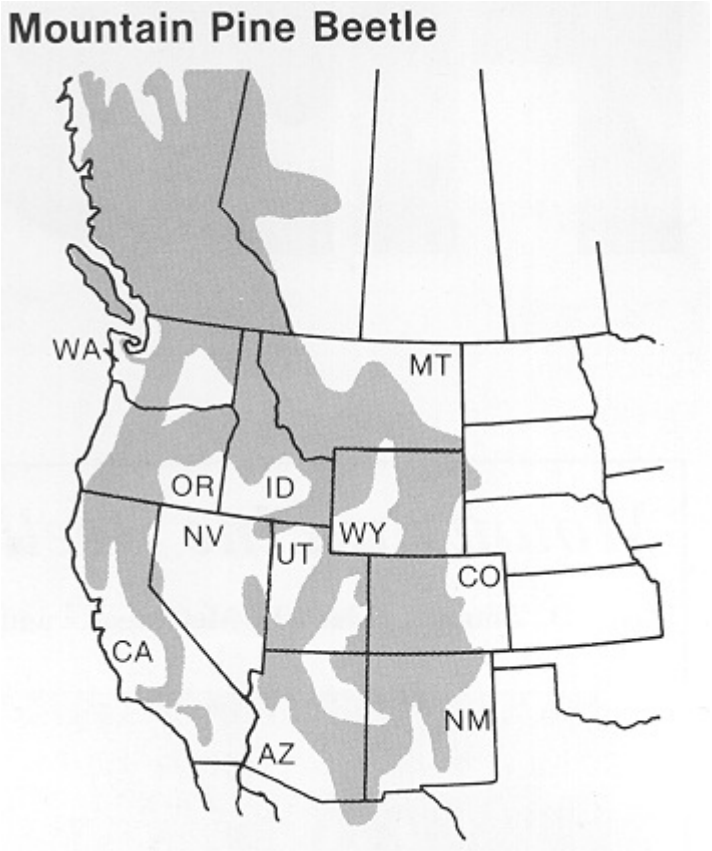

Figure 9. Mountain pine beetle kill across North America (From Amman et al., 2002).

Attacking in the late summer, female beetles (Figure 10) lay eggs in tunnels just beneath the tree's bark. Once the eggs have hatched, beetle larvae (Figure 11) scatter, spreading blue stain fungi which assist in killing pine trees (Leatherman, 2011). As beetles bore into a tree, two types of blue stain fungi (*Ophiostoma clavigerum* and *Ophiostoma montium*) are inoculated into the tree. These fungi attack living cells in the phloem and xylem causing the tree to stop producing resin (Wulder et al., 2006). Additionally, healthy trees may be overcome by beetles attacking in large numbers, termed "mass attack" (Wulder et al., 2006). In either of these circumstances tree's defenses are overcome, resulting in the death of the host tree. Although these insects have short life cycles, living only one year, the damage caused is severe. All pine tree species are suitable hosts for mountain pine beetle, but lodgepole pine seems to be the most "severely impacted," making these trees the primary host for the insect (Wulder et al.,

2006). Because of the relatively large population of lodgepole pine in Colorado, and favorable climate over the last decade, mountain pine beetles have flourished.

Figure 10. Top view of full grown mountain pine beetle (actual size 1/8 to 1/3 inch) (From Leatherman, 2011).

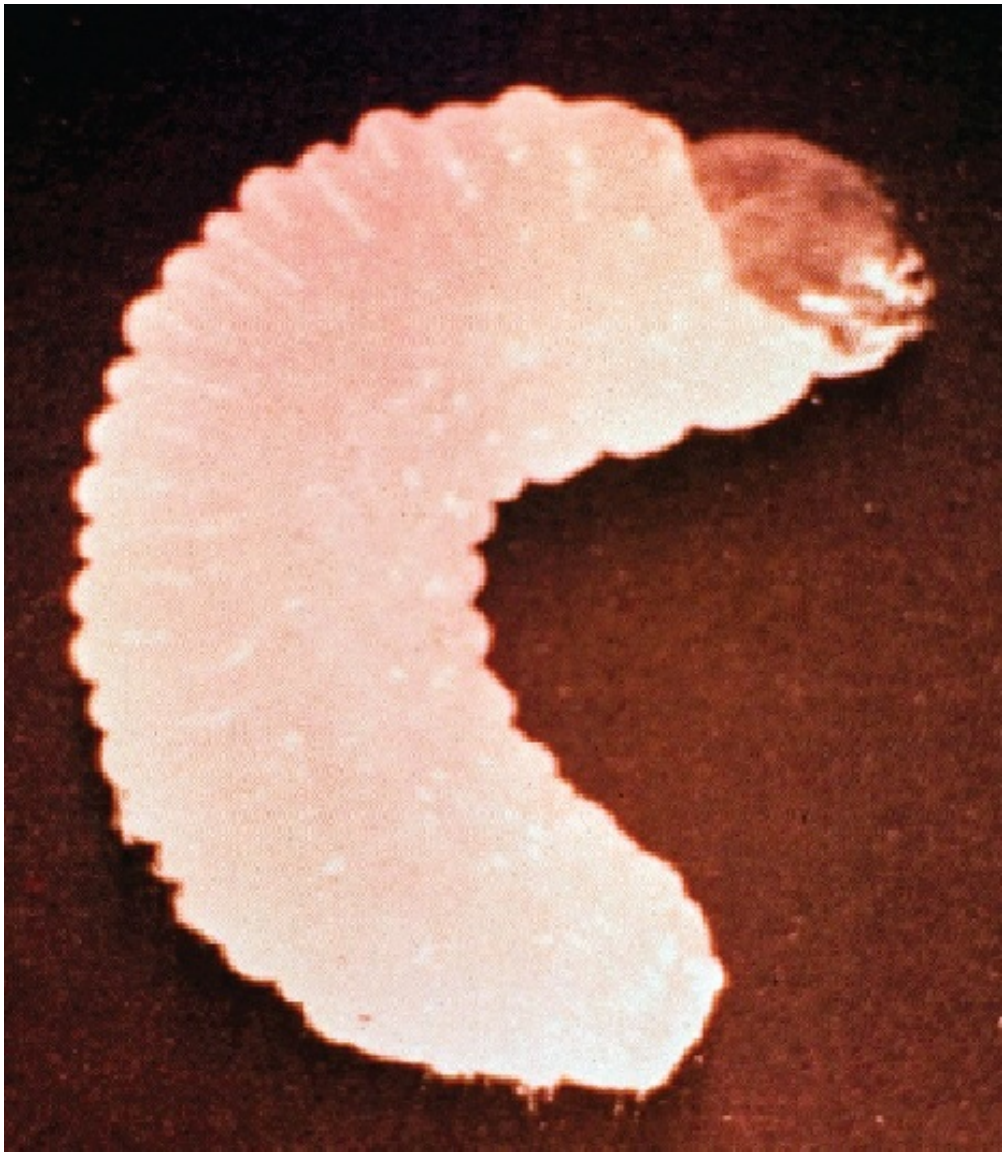

Figure 11. Mountain pine beetle larva (actual size 1/8 to 1/4 inch) (From Leatherman, 2011).

3. Previous Work

There has been an extensive amount of previous work on mapping lodgepole pine degradation due to mountain pine beetle (Skakun et al., 2003; White et al., 2005; DeRose et al., 2011). Skakun et al. used a Tasseled Cap Transformation (TCT) of Landsat-7 ETM+ to obtain wetness indices, which were then used to create an enhanced wetness difference index used to determine patterns in tree stands with known red-attack damage. They determined that sites with larger numbers of red attack trees generated stronger

patterns of red-attack reflectance, those sites having between 30 and 50 trees at red-attack level. Sites with fewer trees in red-attack stage were classified less accurately, due to a smaller number of red crowns, and increased variance due to understory and healthy canopy reflectance factors (Skakun et al., 2003).

Meddens et al. evaluated the classification accuracy of 30 cm spatial resolution multispectral imagery, which was aggregated to coarser resolutions, to assess forest degradation in central Colorado; just south of the area observed for this study. Using Normalized Difference Vegetation Index (NDVI) and Red-Green Index (RGI), results were mapped using a maximum likelihood classifier. Using the 30 cm imagery classification, results were mapped with 87 percent accuracy; but they found that using 2.4-meter spatial resolution imagery the classification accuracy was 90 percent. This difference was attributed to pixels including "more shadow in forested regions than pixels in finer resolution imagery, thereby reducing forest canopy reflectance and allowing improved separation between forest and non-forest classes" (Meddens et al., 2011). Additionally, they found that the 2.4 meter spatial resolution imagery was approximately the size of a tree crown. Ultimately the study showed that using multispectral imagery with spatial resolution of 2.4 meters was best for mapping tree mortality, and that "multispectral imagery can be used to separate multiple post outbreak attack stages (i.e., red-attack and gray-attack) from other classes in the image" (Meddens et al., 2011).

White et al. used aerial imagery of six one-hectare sites in British Columbia. They determined that the aerial imagery was acceptable for use as ground truth with classification accuracy of 99.5 percent. The aerial imagery was then used to validate an unsupervised classification of IKONOS 4-m MSI data. The results showed that red-attacked trees in areas with low-density attack were classified with 54 percent accuracy; while red-attacked trees in areas with medium-density attack were classified with 78 percent accuracy (White et al., 2005).

There is also a wealth of information already available for hyperspectral sensing of forest damage. A study by White et al. used Hyperion data to detect the "relationship between spectral moisture indices and levels of red attack damage" (White, et al., 2007). Moisture indices were generated from the Hyperion data and then compared to the

amount of red attack damage detected in each Hyperion pixel. The results showed that there was good correlation between the Moisture Stress index and the level of red attack damage. The study also showed that it was possible to detect low levels of mountain pine beetle red attack damage over large areas using Hyperion that Landsat does not always detect.

Kumar et al. (2012) used airborne multispectral and hyperspectral data to detect potentially diseased trees over a large area by examining unique spectral signatures. This study used two sets of HSI data from 2007 and 2009, and one MSI dataset from 2009 to map the spread of infection amongst citrus trees in Florida. Through extensive ground truthing to validate the results of the images, and use the use of an image derived spectral library they found that Mixture-Tuned Matched Filtering yielded the greatest accuracy for the mapping results.

The goal of this study was to successfully map the degradation of lodgepole pine trees over time, principally using multispectral data (IKONOS and QuickBird). Airborne Visible/Infrared Imaging Spectrometer (AVIRIS) data were classified using a Mixture-Tuned Matched Filtering approach to produce classification maps utilizing spectral library plots and regions of interest (ROI), to show the degradation of the forest through the years from 2006–2011. Previous studies focused primarily on using one type of data, either MSI or HSI. This study extended the previous work done by showing that through the use of both HSI and MSI data change caused by mountain pine beetle over time could be detected.

THIS PAGE INTENTIONALLY LEFT BLANK

III. METHODS

A. DATA PROCESSING

1. Spatial Adjustments

The QuickBird and AVIRIS images were spatially resized using nearest neighbor resampling to match the IKONOS resolution of 3.7 m for easier comparison between the data sets. Once these images were resized, image chips of the multispectral and hyperspectral images were created where overlapping areas between all images existed. This was done in order to limit the size of the data to be classified, to allow direct comparison, and to make processing times faster. Once these steps were completed, atmospheric corrections were applied to all of the images.

2. Atmospheric Corrections

Remote sensing images need to be atmospherically corrected in order to remove the effects of the Earth's atmosphere. The radiation that returns to a sensor from the Earth's surface changes due to "atmospheric effects caused by molecular and particulate scattering and absorption" (Matthew et al., 2002). Because of these effects it is difficult to compare uncorrected data sets over time. Additionally true reflectance values cannot be obtained without atmospheric correction (Hadjimitsis et al., 2010). For this study, the Fast Line-of-Sight Atmospheric Analysis of Spectral Hypercubes (FLAASH) was used. FLAASH is an atmospheric correction model derived from "'physics-based' mathematics from MODTRAN4" (Cooley et al., 2002). Developed by the Air Force Research Laboratory, Space Vehicles Directorate, Hanscom AFB and Spectral Sciences, Inc. FLAASH was designed to support analyses of visible-to-shortwave infrared hyperspectral and multispectral imaging sensors (Cooley et al., 2002). FLAASH takes properties from the atmosphere and inverts those properties from 'radiance-at-detector' to 'reflectance-at-surface' (Cooley et al., 2002). To make the correction, a radiance image is needed with center coordinates, sensor altitude, ground elevation, pixel size, time and date the image was captured. FLAASH uses standard MODTRAN atmospheric models, which are based on surface air temperature, water vapor, and latitude and longitude.

3. Empirical Line Correction

The data analyzed for this study covered a number of years, and unfortunately, while collected during the same season (summer), were collected in different months. Reflectance values in a single image can vary significantly from target to target based on environmental and observational parameters (Smith & Milton, 1999). While the goal of the atmospheric corrections applied to these data was to produce absolute reflectance that could be compared year-to-year, comparison of FLAASH reflectance spectra for selected (what should be relatively invariant) targets over time again demonstrated significant differences. It was assumed that the reflectance characteristics for these targets should be similar from year-to-year, thus an empirical method was used to accomplish this and gains and offsets were determined to adjust the rest of the data. The so-called "empirical line correction" is a technique for normalizing the reflectance from image to image (Roberts et al., 1986; Gao et al., 2006). This approach requires that at least two targets (usually a bright target and a dark target) be identified and a reference spectrum be measured for each, and then compared to the corresponding data spectrum to determine a linear regression between the two. The result is a set of gains and offsets converting the data spectrum to match the reference spectrum. As used in this research, the 2011 FLAASH-corrected AVIRIS data were used to derive the reference spectra and the 2011 FLAASH-corrected IKONOS spectra were used as the data spectra. In this case, two regions of interest were used (a white roof and an asphalt road), the reflectances for the targets were compared between each of the images and then normalized as above in order to create images with more uniform reflectance (Smith & Milton, 1999). Once the IKONOS reflectance values were matched with the AVIRIS reflectance, the other three MSI images were empirically corrected using a similar approach.

4. Registration

Image to image registration is needed when multiple scenes over the same area are being analyzed for change. Through image to image registration a pixel by pixel comparison is possible (From Richards & Jia, 2005). Ground control points (GCPs) were manually selected across all of the images. GCPs are common points corresponding

to common ground features spread across the images, which allow the images to be registered. A higher number of GCPs typically results in a more accurate registration, depending on the warp method selected (Richards & Jia, 2005). Once GCPs were collected, the images from 2007, 2009, and 2011 were warped to the QuickBird image from 2006 using first degree polynomial warping and nearest neighbor resampling; additionally, the HSI image from 2011 was warped to the 2006 image.

Polynomial image warping is "where the source image coordinates are defined as bivariate polynomials in the destination images coordinates," this is common in remote sensing for image registration and to correct distortions in images (Gustafsson, 1993). Nearest neighbor resampling applies the "pixel that has its center nearest the point located in the image," and is then "transferred to corresponding display grid location" (Richards & Jia, 2005) (Figure 12). Use of nearest neighbor resampling is desirable for spectral analysis applications to avoid changing/biasing the pixel signatures.

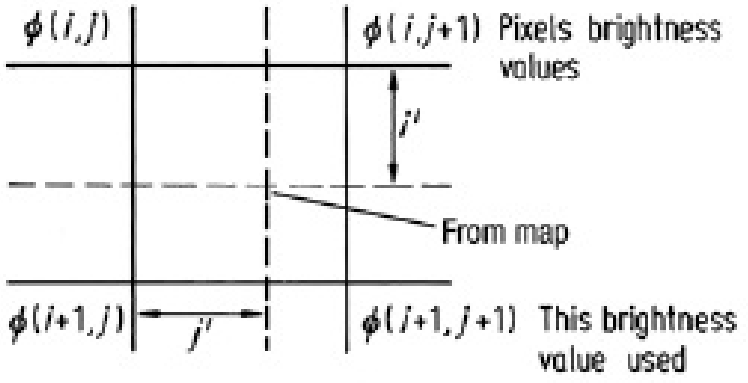

Figure 12. Illustration of nearest neighbor resampling (From Richards & Jia, 2005).

Using the September 2006 QuickBird image as the base image (Figure 13), the other four images, July 2009 from QuickBird, 2007 and 2011 from IKONOS, and 2011 from AVIRIS, were warped using first degree polynomial warping and nearest neighbor resampling (Figures 14 & Figure 15). GCPs were collected throughout the 2007, 2009, and the MSI and HSI 2011 images, and were used to warp to match the image from 2006. This results in a warped file and an estimate of root mean square (RMS) error. RMS error

is an overall estimate of the accuracy of the mapping, computed by taking the root mean square of all the residuals in both easting and northing directions (Richards & Jia, 2005). For the MSI scenes, common features were easier to identify, and more GCPs were found. Between the QuickBird 2006 image and the IKONOS 2007 image 16 GCPs were used, which led to a RMS error of 0.024 pixels. 19 GCPs were used to warp the 2006 and 2009 QuickBird scenes, giving a RMS error of 0.007 pixels. Between the 2006 QuickBird and 2011 IKONOS 17 GCPs were used and a RMS error of 0.056 pixels was the result. Finally, between the 2006 QuickBird and the 2011 AVIRIS scenes 12 GCPs were used, this resulted in a RMS error of 0.18 pixels. Based on the low RMS error for all the images the registrations were acceptable.

Figure 13. Spatially adjusted, atmospherically and empirically corrected QuickBird September 2006. Image size is 5.952 km by 2.62 km.

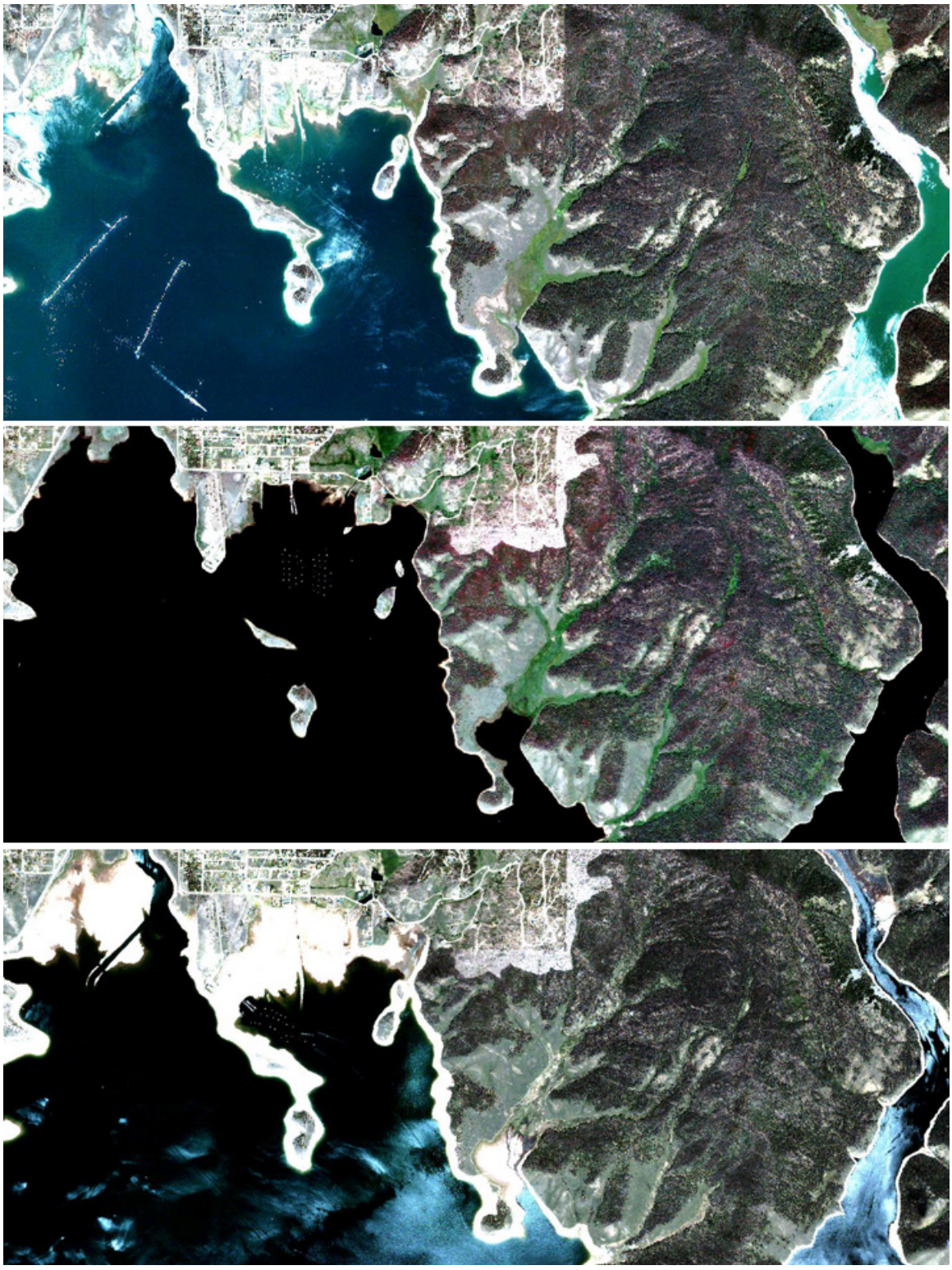

Figure 14. Spatially adjusted, atmospherically corrected, and registered MSI images of study area. Progressing downward, the images are August 2007 IKONOS, July 2009 QuickBird, and June 2011 IKONOS. Image size is 5.952 km by 2.62 km.

Figure 15. Spatially adjusted, atmospherically and empirically corrected, and registered AVIRIS image of study area from 2011. Image size is 5.952 km by 2.62 km.

5. Band Masks

The site chosen for this study has an abundance of water (Lake Granby, Colorado). Areas with more tree coverage and less water would obviously be preferable, but due to the limited availability of overlapping data this site was the most usable. In order to negate the influence of the water, band masks were created from regions of interest (ROI) from the 2011 AVIRIS true color image that masked the water out of the scenes and allowed for more accurate results. The data were also masked to exclude green vegetation that was clearly "not trees"; a band mask was created for green grass, also done by selecting ROIs that covered those areas in the true color image.

6. Spectral Analysis

Once these processes were completed, the data were analyzed using an approach based on reduction of spectral and spatial dimensionality and linear spectral mixing using image or spectral library spectra (Boardman & Kruse, 2011). The "Spectral Hourglass" is a multi-step process that can be applied to either hyperspectral or multispectral data and includes everything from atmospherically correcting data to producing classified image results (Figure 15). Using this approach allowed for "consistent ways to extract spectral

information from hyperspectral data without *a priori* knowledge or requiring ground observations" (Kruse & Perry, 2009).

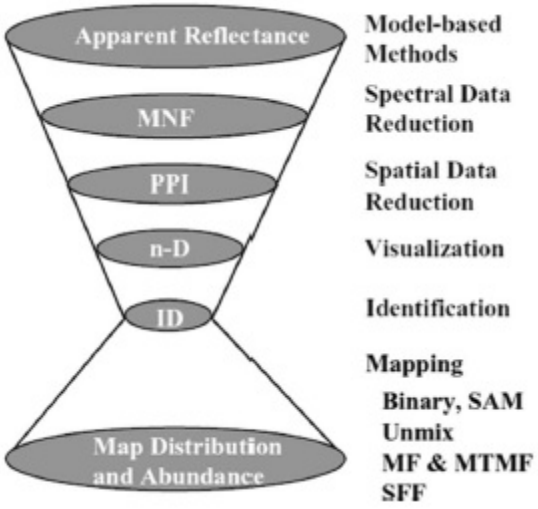

Figure 16. Spectral hourglass method for processing and classifying data (From Boardman & Kruse, 2011).

The approach typically uses the data themselves to find and map image spectral endmembers, those unique spectral signatures that define the components of an image. This is accomplished by first reducing the spatial size of the input imagery of the spectral data through the minimum noise fraction (MNF). The MNF is a transform of the spectral data that is used to determine the inherent dimensionality of the data to segregate noise (Green et al., 1988; Boardman & Kruse, 2011). MNF is similar to Principal Components Analysis (PCA), however, rather than a linear transformation that orders the output data by variance, MNF orders the data based on signal-to-noise ratio (SNR), the highest SNR showing in the first tens of bands (Boardman & Kruse, 2011). For this study, thirty out of a possible 205 MNF bands of AVIRIS data were used and all four bands of the MSI data were used. The number of useful bands was determined based on Eigenvalue plots, which relate the higher Eigenvalue numbers to bands with higher SNR (Boardman & Kruse, 2011).

After determining the number of spectral bands to use for analysis, endmembers can be derived from the imagery or they may be selected from user supplied image ROIs

or spectral libraries. This study used both a spectral library and ROIs. The spectral library of nine averaged known endmembers consisted of young green trees, two stages of green healthy trees, green infected trees, partially infected trees with green and red needles, three stages of red beetle kill trees, and trees with beetle kill with gray bark (Figure 16). These spectra show features commonly found in healthy and unhealthy lodgepole pine trees. The spectral library was resampled to match the wavelengths and values of both the HSI and MSI images and classification was performed (see below).

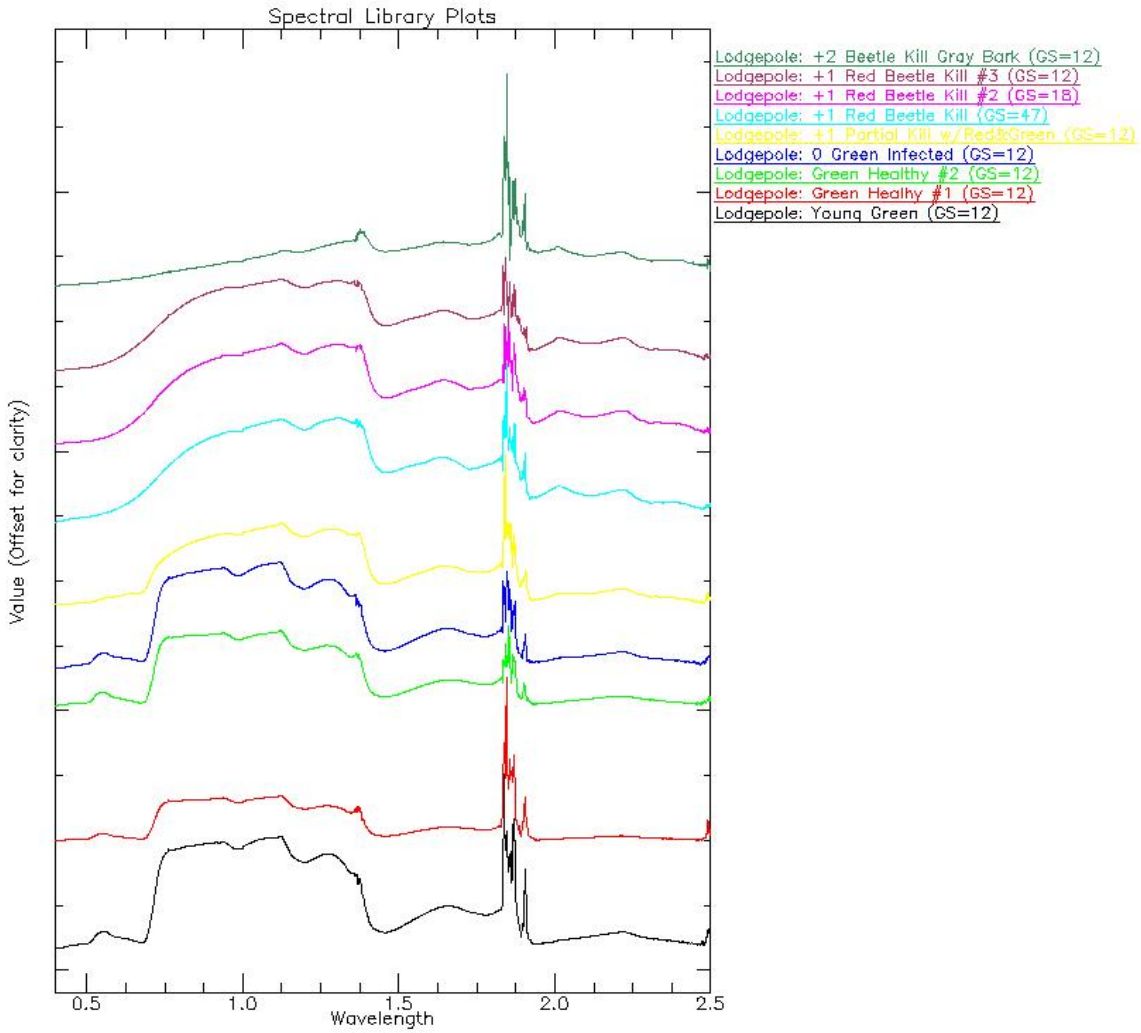

Figure 17. Spectral library of averaged endmembers of tree degradation from young green to beetle kill with gray bark (Kruse 2008, unpublished data).

In addition to the spectral-library-based method, the image ROI approach was used with three ROIs created by examining the spectral signatures of pixels within the AVIRIS data; green healthy, red kill, and gray kill. Because all the data sets were coregistered, the ROIs found in the AVIRIS data matched the multispectral data. AVIRIS data were found to be the most logical to extract ROIs from based on the higher spectral resolution.

Based on the goal of finding pixels matching ROI or library spectral signatures for lodgepole pine trees at different stages of health, Mixture-Tuned Matched Filtering (MTMF) was selected for spectral mapping of these data. Other classification methods (maximum likelihood, Mahalanobis distance) were tested and rejected for this research because the MTMF approach appeared to be most sensitive to the vegetation differences. MTMF is a "partial linear unmixing used to spectrally unmix the data and to accurately map the apparent abundance of a known target material in the presence of a composite background" (Boardman & Kruse, 2011). HSI is used for a variety of mapping applications, but the pixels in HSI scenes are often spectrally mixed. Spectral mixing is the mixing of different materials within a single pixel (Boardman & Kruse, 2011). In order to find the purest endmembers in a scene the pixels then need to be unmixed. To unmix the data it is necessary to calculate the fractional abundance of each endmember of each pixel in the scene based on the known endmembers and the scene spectra (Boardman & Kruse, 2011). Known endmembers come from analysts' knowledge of an area in a scene, or from spectral libraries of specific endmembers (Boardman & Kruse, 2011).

In order to create the MTMF results the algorithm uses a matched filter (MF) to maximize the response of the known endmember and suppresses the response of the composite background (the covariance of all other endmembers), thus matching the known signature. MF was designed for target signal detection, and has been called the "optimal linear detection method for locating a known signature in the presence of a mixed and unknown background" (Boardman & Kruse, 2011). The MF uses the calculation of linear operator or projection vector to balance target detection and background suppression (Boardman & Kruse, 2011). The target that is distinguishable

from the background is heavily weighted against the background, and the portion of the target that is indistinguishable from the background is suppressed, allowing for identification of target materials (Boardman & Kruse, 2011); see Figure 17.

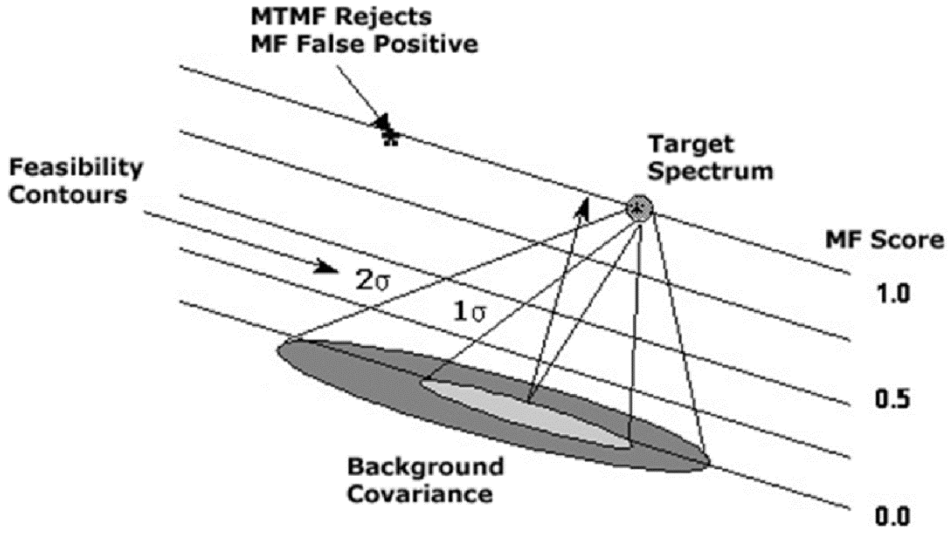

Figure 18. Illustration of MTMF concept (From Boardman and Kruse, 2011).

This technique was useful for the purposes of this study because it required no knowledge of the area or the endmembers, and the resulting output is easily explainable by physical processes of materials as illustrated by their spectra. The background values of the MF images will be lower than the known endmembers, and appear as darker pixels in the MF images as seen in Figure 18. Additionally, the MTMF process creates infeasibility images that are used to reduce the number of false positives that can occur when only using MF images. The infeasibility results display pixels that contain the target material and the background in terms of noise standard deviations. The lower the infeasibility score, the higher the probability that the material is a feasible mixture of the target spectrum and the background materials (Boardman & Kruse, 2011).

IV. RESULTS

A. SPECTRAL MAPPING RESULTS

MTMF results provide "high-performance subpixel target detection and extreme false alarm rejection," making MTMF a very reliable method of spectral mapping (Boardman & Kruse, 2011). Because MTMF is using two sets of information (the MF score and the Infeasibility), the final result shows whether a pixel is a feasible mixture of the target and background, and the estimated abundance of the target occurring in that pixel (Boardman & Kruse, 2011). The MTMF approach was first applied using the spectral library endmembers, and then separately using the image ROI endmembers for comparison. Only the most feasible, best MF matches are shown in the results images.

1. Matched Filter (MF) Score Results

Two sets of MF results were generated as part of the MTMF processing using the aforementioned spectral library and image ROIs. Separate MF images for each of the nine library spectra and the three ROIs were produced for all five data sets. The MF score images show areas with higher MF scores as brighter pixels, pointing to areas with large abundance where the target material likely occurs. Figure 19 shows the MF image created by comparing the library spectrum of young green lodgepole pine to the pixel spectra of the QuickBird image from September 2006. The brighter areas suggest young green lodgepole pine trees inhabit those pixels. Based on examination and comparison with true-color imagery, however, areas with the brightest pixels do not appear to all be young tree growth; rather many of these are green grassy areas. This occurred because the spectra for green grass and young green lodgepole pine are very similar; these areas were masked from further analysis. Figure 20 shows the MF image created by comparing the image ROI average spectrum for green healthy trees to the pixel spectra. The differences between the images derived using the two different sources of endmember spectra are clear. Many more pixels were considered green healthy, brighter, in the ROI MF image. However, there is still confusion in the ROI MF image in the grassy areas.

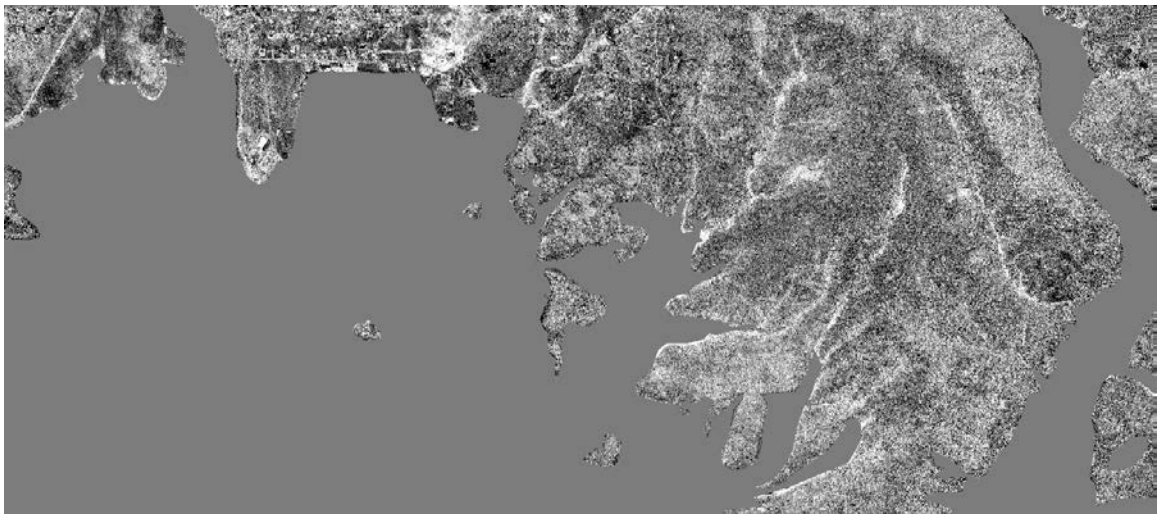

Figure 19. MF score of young green lodgepole pine trees from September 2006 QuickBird data created by comparing image pixels to library spectra. Image size is 5.952 km by 2.62 km.

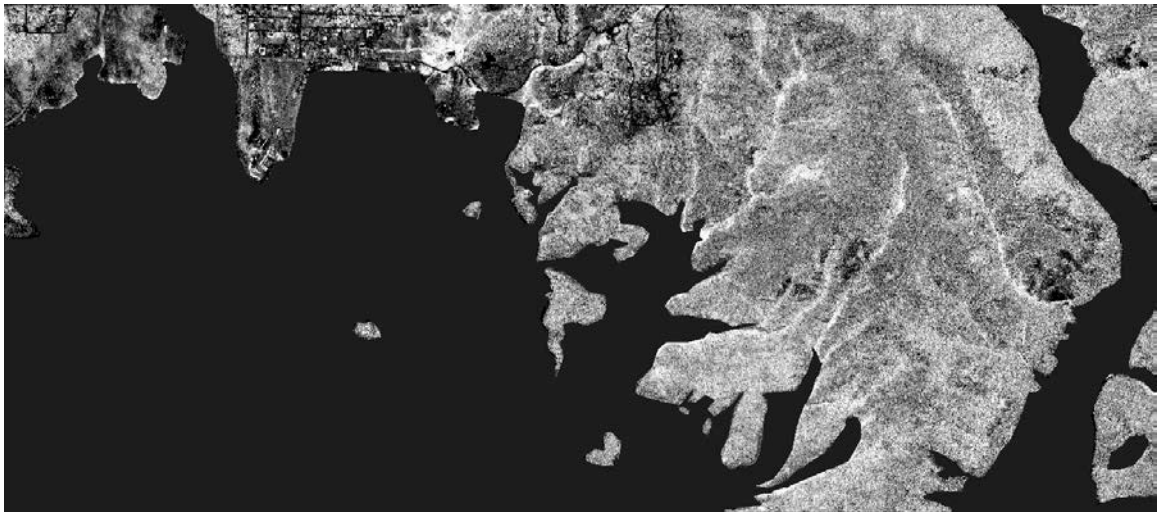

Figure 20. MF Score of green healthy lodgepole pine trees from September 2006 QuickBird data created by comparing image pixels to regions of interest. Image size is 5.952 km by 2.62 km.

2. Infeasibility Results

MTMF infeasibility images help to remove false positive pixels, those pixels that had high MF scores but are unlikely to be the target material based on the mixture of the target spectrum and the background distribution (Boardman & Kruse, 2011). Infeasibility images corresponding to the MF score images were created for each data set. The

infeasibility images from the 2006 QuickBird data, created by comparing both spectral library plots and ROIs to spectrum from image pixels (Figure 21 & Figure 22), show that the brighter areas in the MF score image are not necessarily young lodgepole pine trees, but many are rather false positives in the MF score image.

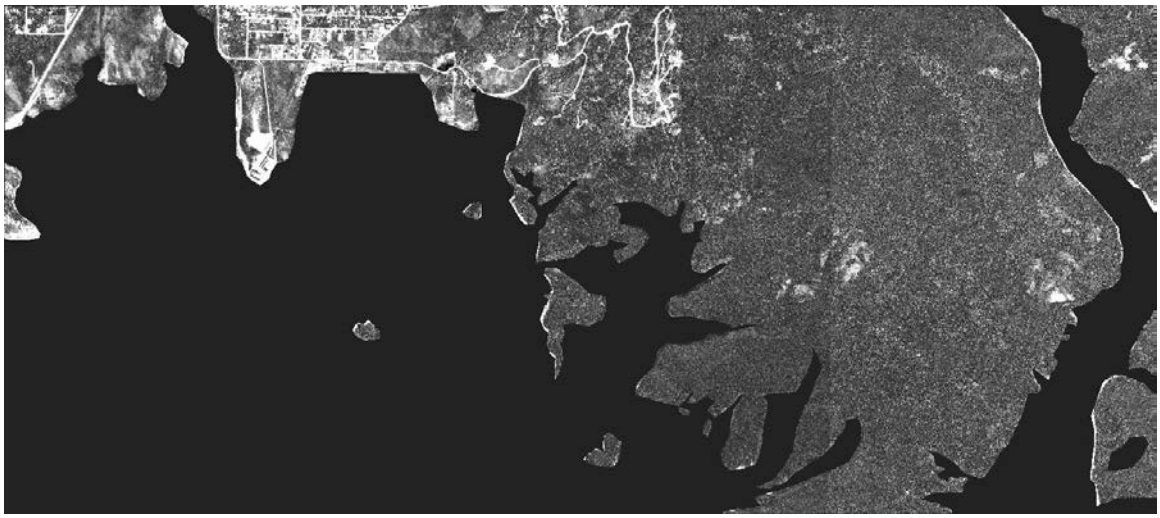

Figure 21. Infeasibility image of young green lodgepole pine trees from September 2006 QuickBird data created by comparing image pixels to library spectra. Image size is 5.952 km by 2.62 km.

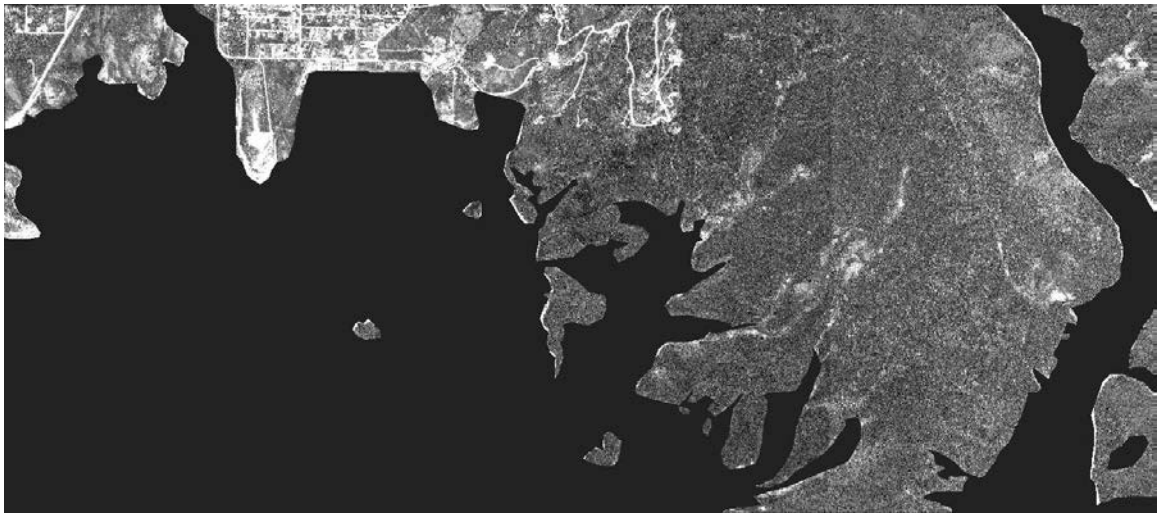

Figure 22. Infeasibility image of green healthy lodgepole pine trees from September 2006 QuickBird data created by comparing image pixels to regions of interest. Image size is 5.952 km by 2.62 km.

Visual examination of the MF score and infeasibility images together can be used to show where young green lodgepole growth (if any) occurred. More typically, however, an interactive process performed using 2D scatterplots is used to discriminate these areas (Figure 23) (Boardman & Kruse, 2011). The 2D scatterplot plots MF score against infeasibility. Pixels with high MF scores and low infeasibility (pixels colored green) are in the lower right corner of the scatterplot. These pixels represent the most likely areas of young green lodgepole pine tree growth in the September 2006 QuickBird image (Figure 24).

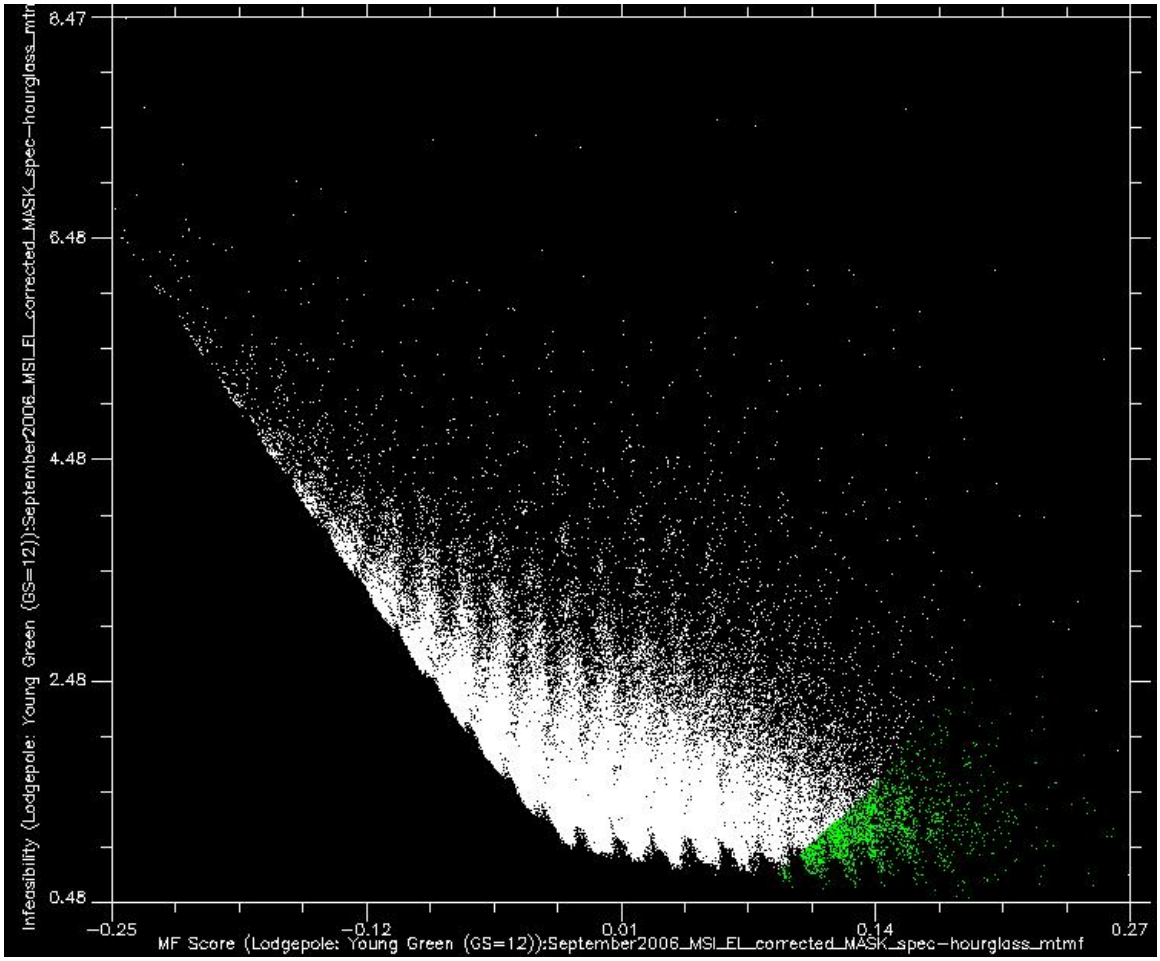

Figure 23. 2D scatterplot of young green lodgepole pine with MF score along the x-axis and infeasibility along the y-axis. Green pixels represent the highest MF score and lowest infeasibility in the September 2006 QuickBird using library endmembers.

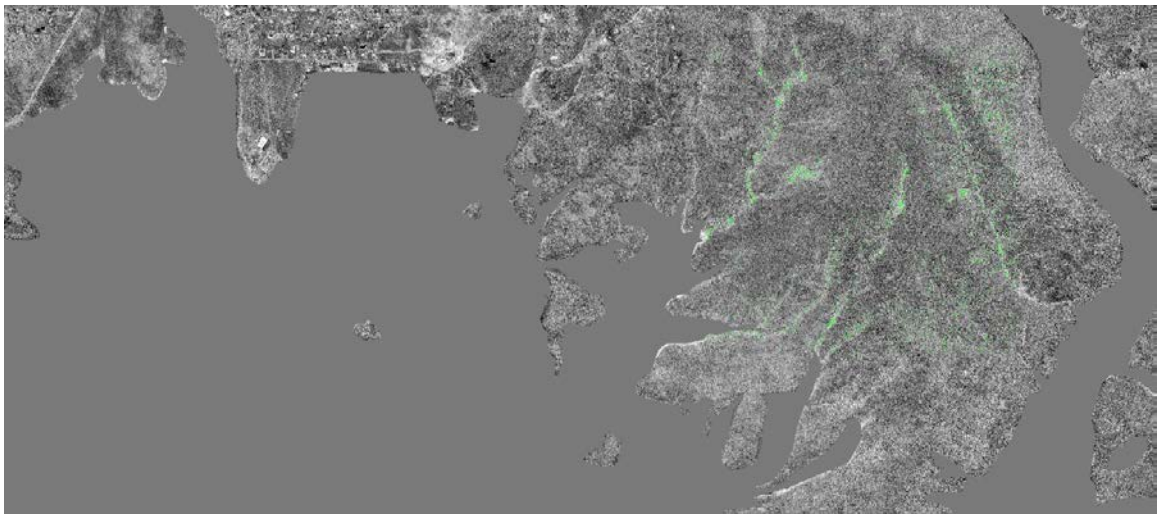

Figure 24. Green pixels from the 2D scatterplot overlaid on MF score image from September 2006 QuickBird data. Green pixels represent areas were likely young green lodgepole pine trees exist. Image size is 5.952 km by 2.62 km.

3. MTMF Ratio Results

MTMF/Infeasibility ratioing is an approach that can be used to automate the MTMF analysis in a consistent fashion for multiple images. The MTMF ratio images highlight pixels most likely to contain the target material. This approach has been successfully used for analysis of imaging spectrometer data for mineralogy (Kruse et al., 2011). The MTMF Ratio results for this research were created by dividing the MF score images by their corresponding infeasibility images. Figure 25 shows an example of the MTMF ratio for the library spectra to image pixel spectra comparison, from the September 2006 QuickBird data. The resulting MTMF Ratio image shows areas with high abundance of young green lodgepole pine trees as brighter pixels, while suppressing the pixels that were classified falsely as young green lodgepole pine. There is still minor confusion among the grassy areas that were not masked in this image, but much of what was falsely classified as young green lodgepole pine in the MF score image has now been correctly suppressed.

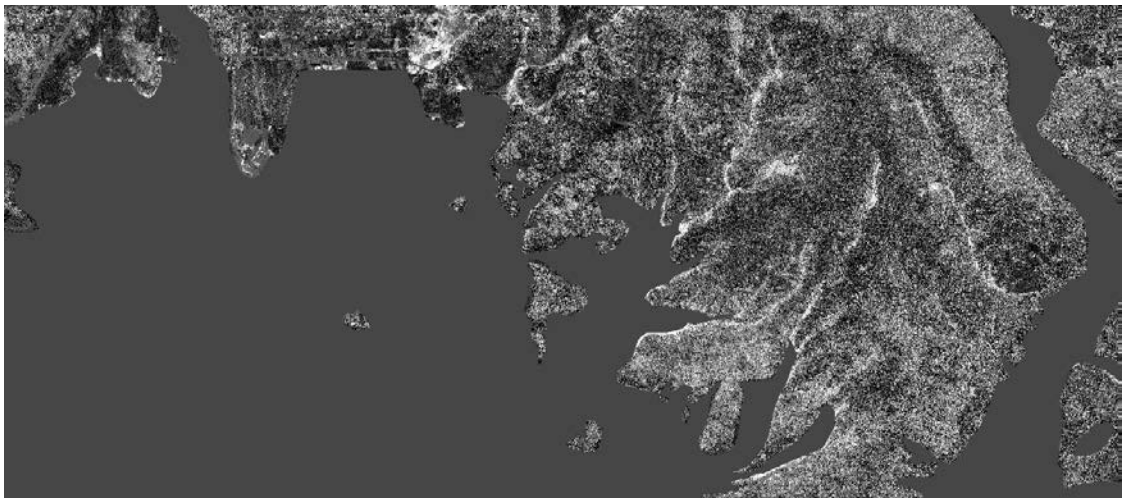

Figure 25. MTMF ratio image of young green lodgepole pine trees from September 2006 QuickBird data created by comparing library spectra to image pixels. Image size is 5.952 km by 2.62 km.

Figure 26 shows the MTMF ratio result created by comparing the three ROIs to image pixel spectra. The differences between the classifications using the two difference endmember sources are fairly obvious. The ROI MTMF ratio image shows much more green healthy lodgepole pine than the spectral library MTMF ratio image. The spectral library image confused grassy areas as young green lodgepole pine, while the grassy areas in the ROI image were suppressed.

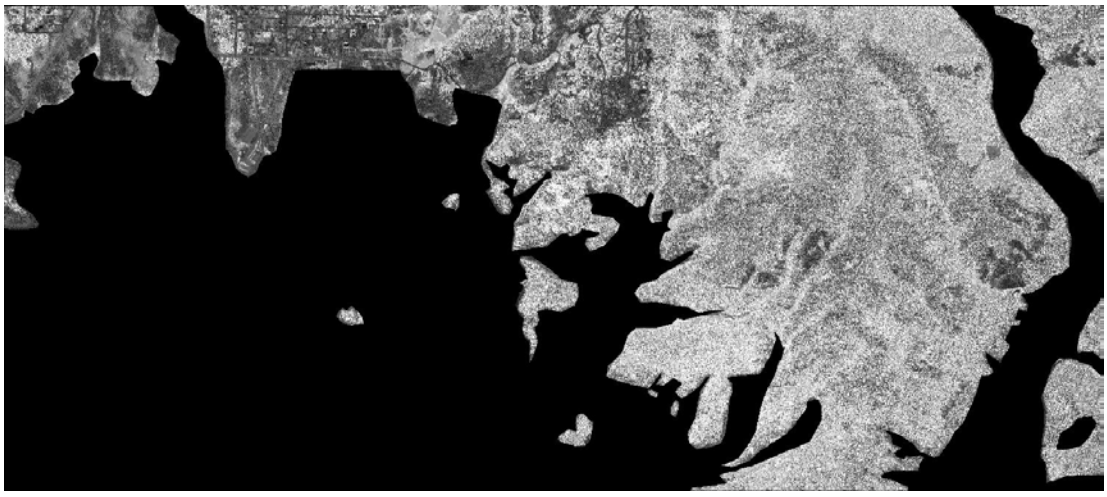

Figure 26. MTMF ratio image of green healthy trees from September 2006 QuickBird data created by comparing image pixel spectra to regions of interest. Image size is 5.952 km by 2.62 km.

Classification maps were created from the MTMF ratio images by determining a threshold, found by comparing the MF versus infeasibility ratio image histograms. Using interactive stretching to manipulate the brightness of the image ensures that pixels that remain bright are the most likely to be the target material. By examining the histograms, a common threshold was found between all the years of MTMF ratio data. To maintain consistency through the classification process, it is important to use the same threshold, otherwise the results will differ from year to year. The threshold used for the spectral library classified images was 0.052, for the data classified using the three ROIs the threshold was 0.444 (Figure 27).

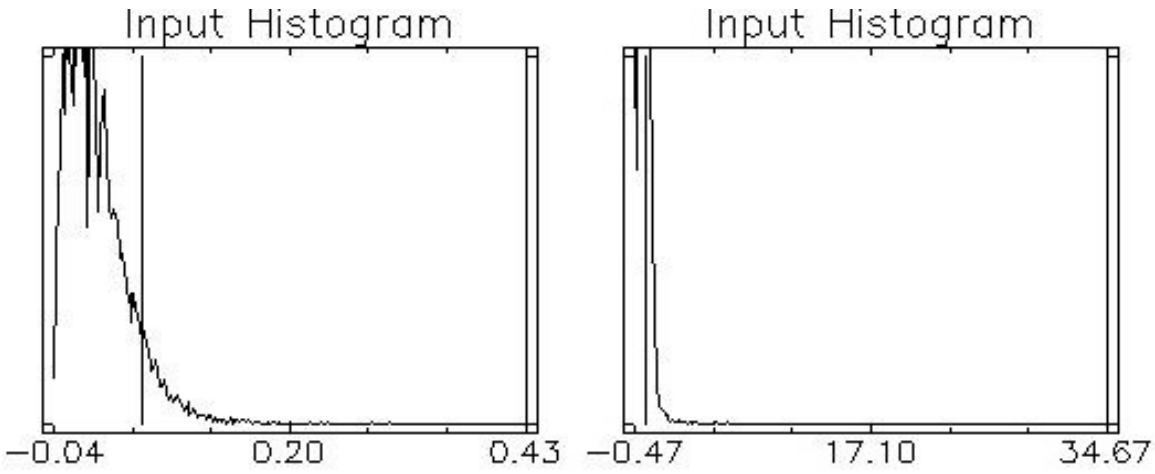

Figure 27. Histograms for September 2006 QuickBird data. Histogram on the left is the spectral library classified histogram. Histogram on the right is the ROI classified histogram.

Figure 28 shows an example of the MTMF ratio classification results for the 2006 QuickBird data showing the best matches to the spectral library endmembers. Once the classification maps were created it was clear that the multispectral imagery did not have high enough spectral resolution to map all the endmembers present in the spectral library. Figure 28, the original MTMF ratio classification image, created by comparing the spectral library to image pixel spectra from September 2006, classified most of the scene as partial kill trees with red and green needles.

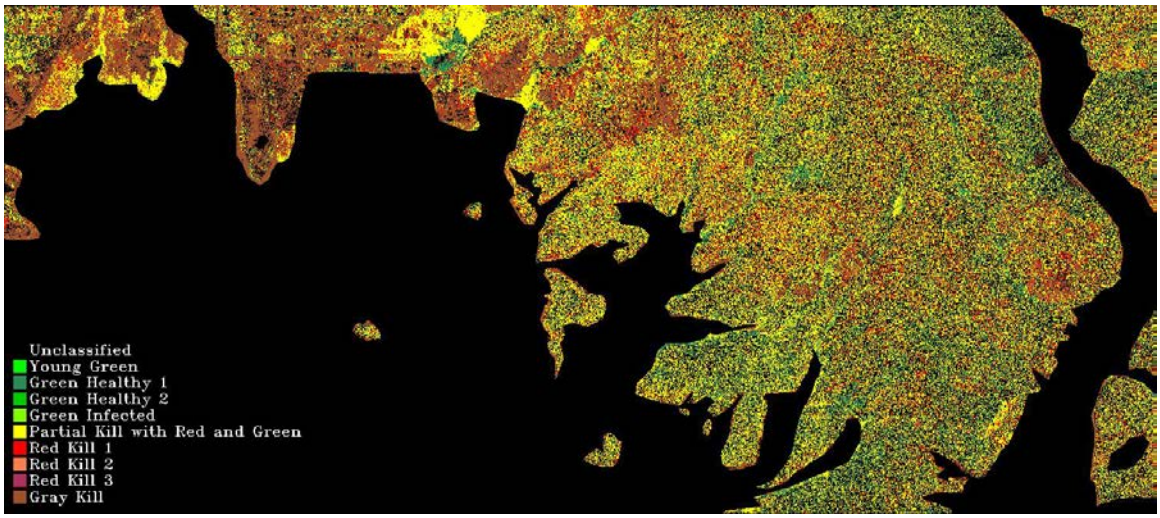

Figure 28. Original MTMF ratio classification map from September 2006 QuickBird data. This image was created by comparing library spectra to image pixel spectra. Most of the terrain is classified as partial kill trees with red and green needles. Image size is 5.952 km by 2.62 km.

4. Combined Classes

Examining the spectral library, it was evident that there was not much difference between the spectrum for partial kill with red and green needles and the spectra for the three other classes of red beetle kill trees (Figure 29). Further examination of the spectral library found that the spectra for the three green classes were not much different than the spectrum for green infected trees (Figure 30).

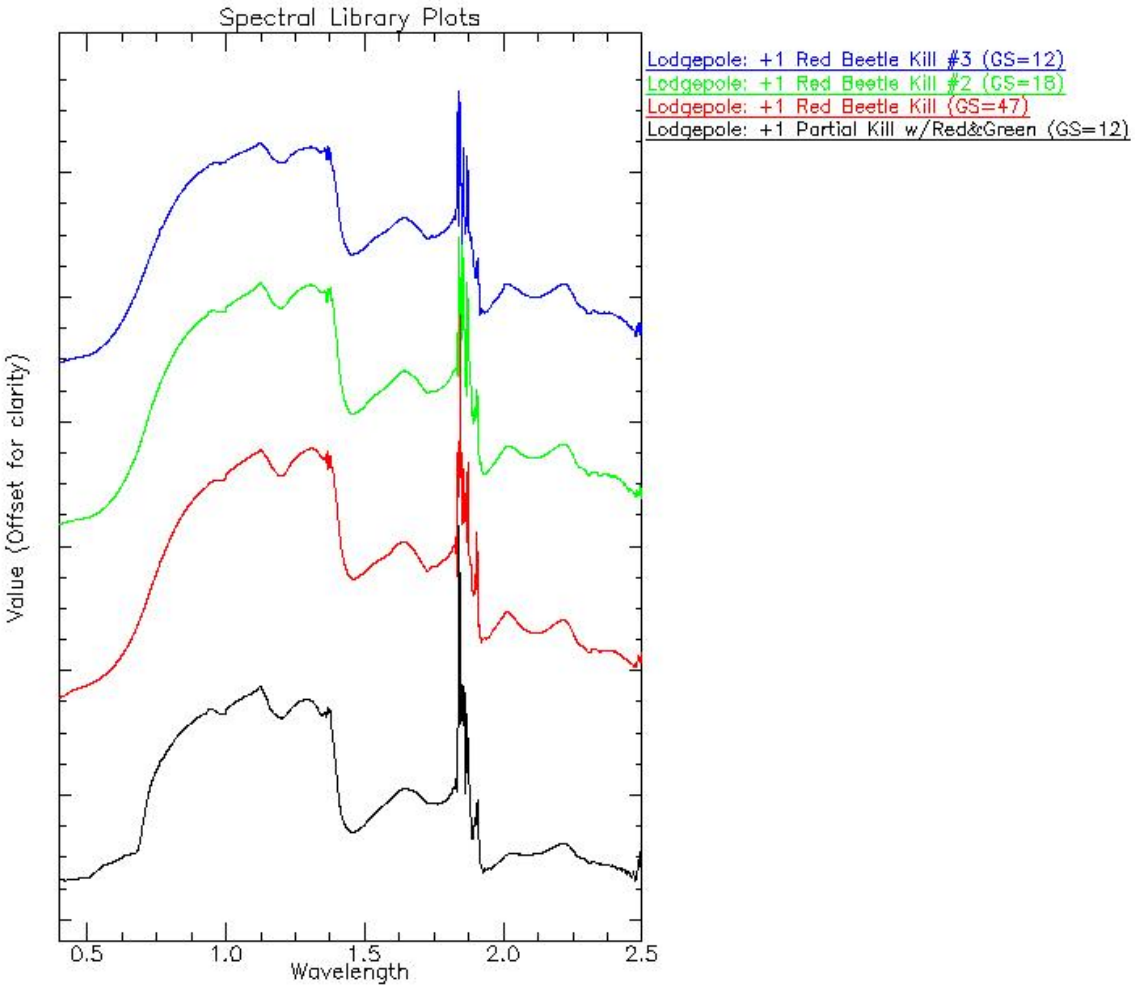

Figure 29. Spectra for three classes red beetle kill trees and one class for partial kill trees with red and green needles. The differences between the spectra were not significant enough to map to multispectral imagery.

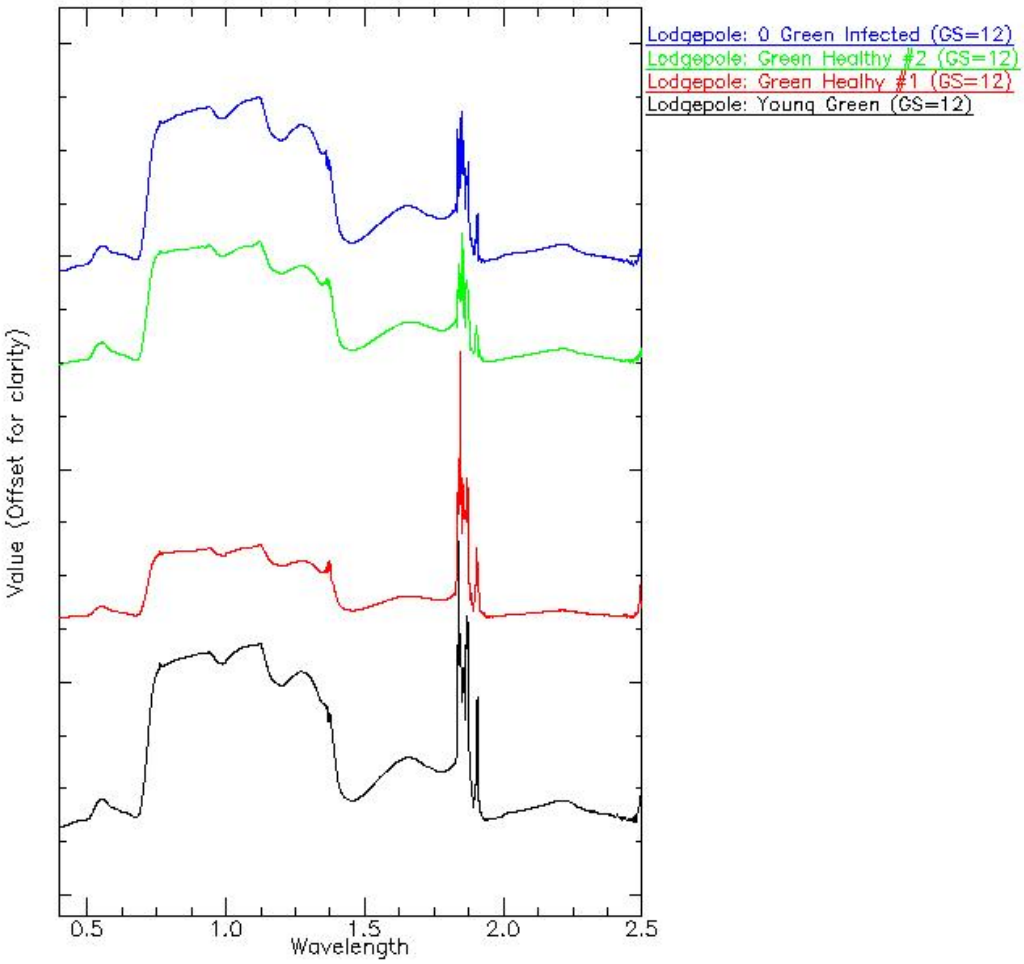

Figure 30. Spectra for three classes of green healthy trees and for one class of green infected trees. The differences between the spectra were not significant enough to map to multispectral imagery.

Recognizing that the spectral changes between these endmembers were subtle, the classes were merged in order to create more distinctly different classification maps. From the nine spectra used in the original classification attempt, three classes remained: green healthy, red kill, and gray kill. Merging the classes made visual analysis easier, and showed more change over time. Figure 31 shows the classification using the merged spectral library classes. Using the merged classes, most of the area was classified as either red or gray beetle kill. In September 2006 most of this area had already been significantly killed off. There are pockets of healthy trees, but at this point most of the trees were already decaying.

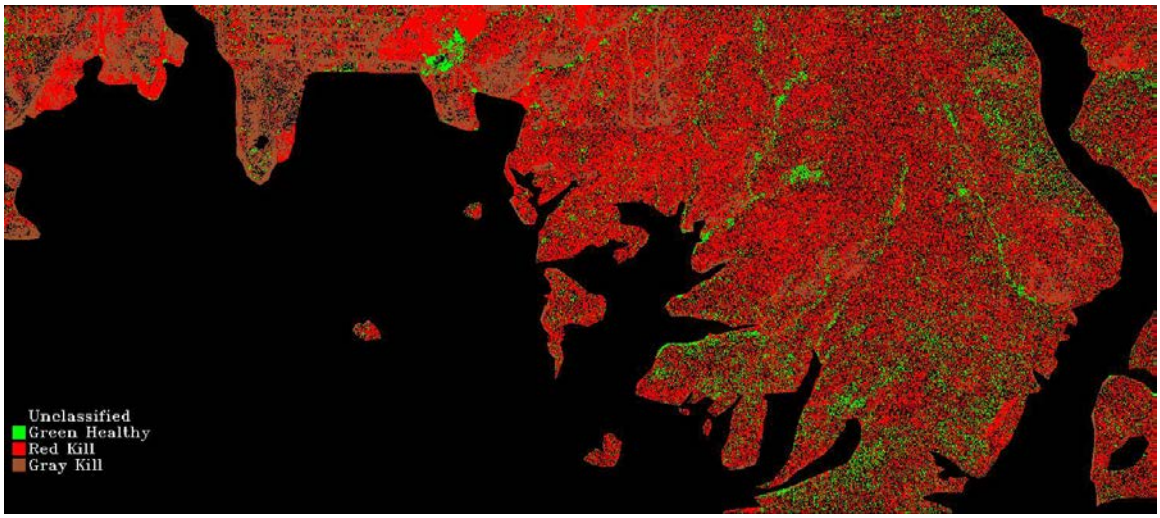

Figure 31. MTMF ratio classification map comparing library spectra to image pixel spectra from September 2006 QuickBird data. Note that most of what was classified as partial kill trees with red and green needles is now classified as red beetle kill. Image size is 5.952 km by 2.62 km.

B. MULTI-YEAR COMPARISONS FOR CHANGE DETECTION

With the endmembers merged into three classes, classification maps for each year of data were created. In order to detect change between the images, visual comparisons were made, as well as mathematical comparisons via confusion matrices and plots of selected confusion matrix parameters.

1. Visual Comparison of the MTMF Results over Time

a. Comparison of Classification Maps Created from Library Spectra

Figures 31, 32, 33, and 34 show the results of the classification maps created by comparing spectral library plots to image pixel spectra. Figure 31 (above) is the September 2006 QuickBird classification. The classified maps were all created using the same MTMF ratio threshold of 0.052 as described previously. The colors used for the map represent the different stages of health among the trees in the forest (green for healthy trees, red for red beetle kill trees, and brown for wholly dead trees). Looking at the classified maps it is clear that the trees in the forest are dying. With the exception of 2009, which was a wet year following another wet year (Colorado Climate Center

Colorado State University, 2012), the progression of the maps shows expected patterns as beetle infestation spreads over time. Additionally, some green areas in the 2009 classification image represent grassy areas that were not fully masked out of the whole image. Those areas are present in the other classification maps; however, the rainfall for the other years was not as high, resulting in dryer grass in the valleys (Colorado Climate Center Colorado State University, 2012). The amount of green goes down significantly from 2006 to 2011. The progression of mountain pine beetle is evident from the MTMF ratio classification results. Based on the life cycle of mountain pine beetle the results from 2006 to 2007 should show significantly more red beetle kill trees; through visual interpretation this seems to be the case. The green areas are not as abundant in the 2007 classification; the grassy areas that appear in the 2006 classification were classified as red in 2007, which given the lack of precipitation during the water year should be the case.

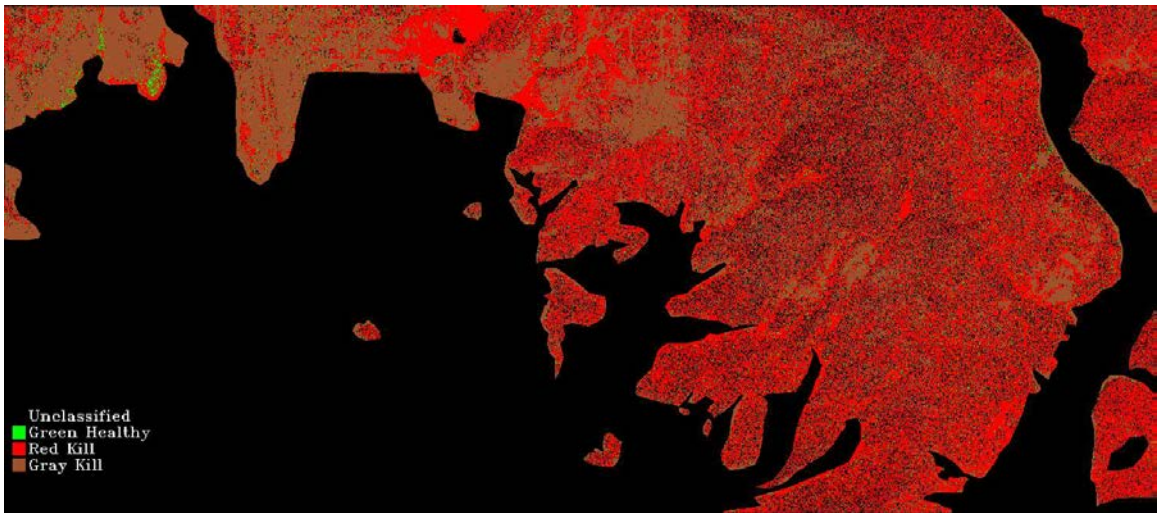

Figure 32. MTMF ratio classification map from August 2007 IKONOS data created by matching spectral library plots to image pixel spectra. Image size is 5.952 km by 2.62 km

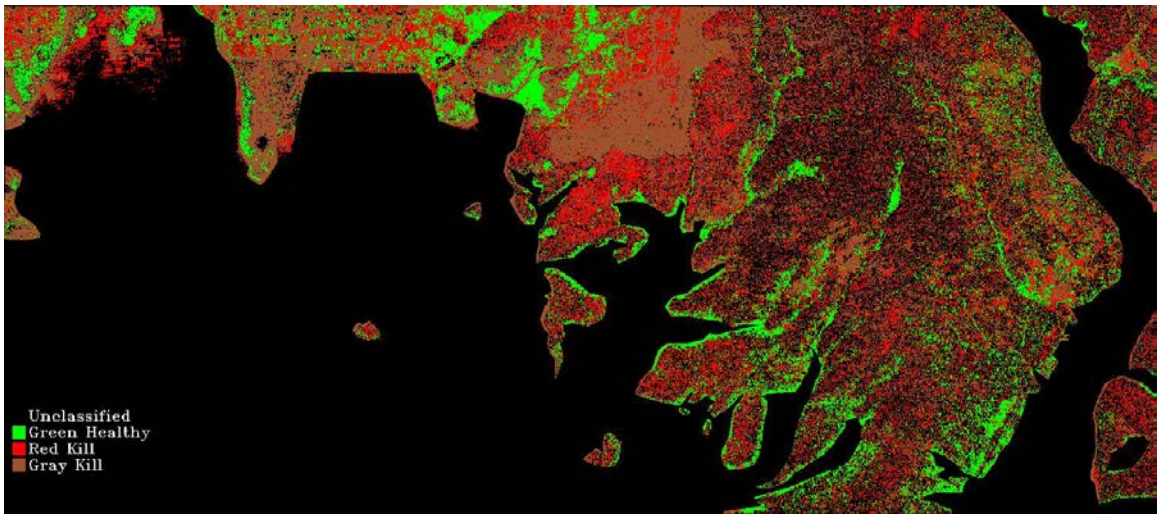

Figure 33. MTMF ratio classification map from July 2009 QuickBird data created by matching spectral library plots to image pixel spectra. Image size is 5.952 km by 2.62 km

Figure 34. MTMF ratio classification map from June 2011 IKONOS data created by matching spectral library plots to image pixel spectra. Image size is 5.952 km by 2.62 km

Overall, the classification appears to be successful, showing less green healthy pine in June 2011 than in September 2006. The progression from green, to red, to brown is visually evident in this classification attempt. Remembering that in 2008 and 2009 precipitation in the area was well over normal (Colorado Climate Center Colorado

State University, 2012), the classification of the 2009 data should also be considered successful, but not representative of the tree decline.

Comparing the 2007 and 2009 classifications, the transition from red to brown is seen; additionally, comparing the 2009 and 2011 classifications the turn from green, to red, to brown is even clearer. The decline of the forest can be seen visually by comparing the results from the MTMF ratio classification maps that were created using the spectral library.

Classification maps were also created using the library spectra for the 2011 AVIRIS data (Figure 35). Visually the two maps from 2011 should match fairly closely; otherwise the classification results would have been incorrect. Comparing the two shows that the classified areas in both images matched relatively well, though the AVIRIS data show fewer red kill and more gray kill (brown).

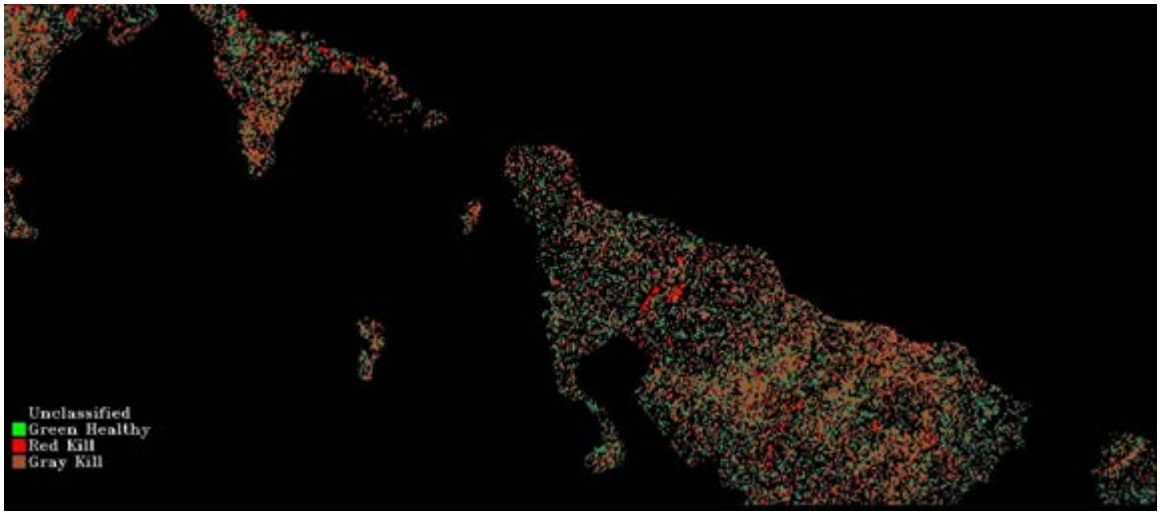

Figure 35. MTMF ratio classification map created by matching library spectra to image pixel spectra from August 2011 AVIRIS data. Image size is 5.952 km by 2.62 km

b. Comparison of Classification Maps Created from Regions of Interest

The results of the classified images mapped by comparing ROIs to image pixel spectra differed somewhat from the results created by using library spectra. Figures 36, 37, 38, and 39 show the results of the MTMF ratio classification using ROIs. Three

regions of interest were used to create the classified images (green healthy, red kill, and gray kill). Figure 36 is the September 2006 classification created by using the three ROIs, followed by the August 2007, July 2009, and June 2011. Using a threshold of 0.444, found as described previously by stretching the histogram of the MTMF ratio images, produced the ROI classification results.

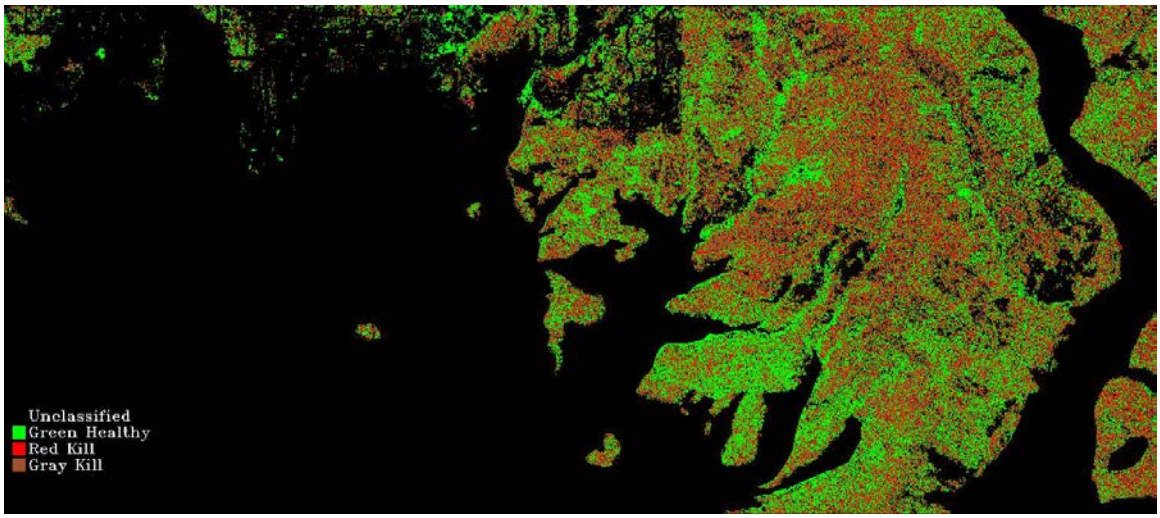

Figure 36. MTMF ratio classification map from September 2006 QuickBird data created by matching regions of interest to image pixel spectra. Image size is 5.952 km by 2.62 km

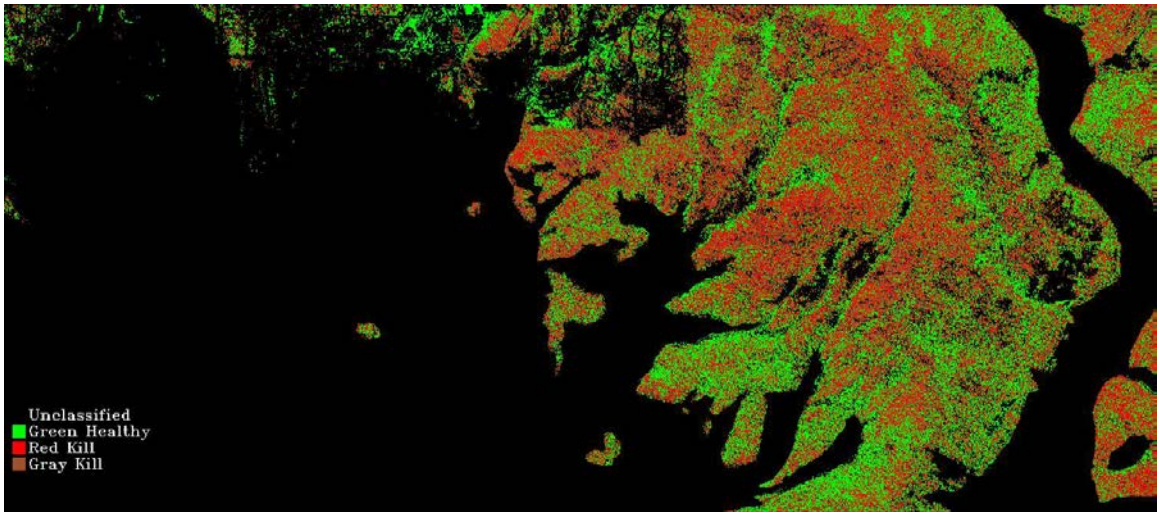

Figure 37. MTMF ratio classification map from August 2007 IKONOS data created by matching regions of interest to image pixel spectra. Image size is 5.952 km by 2.62 km.

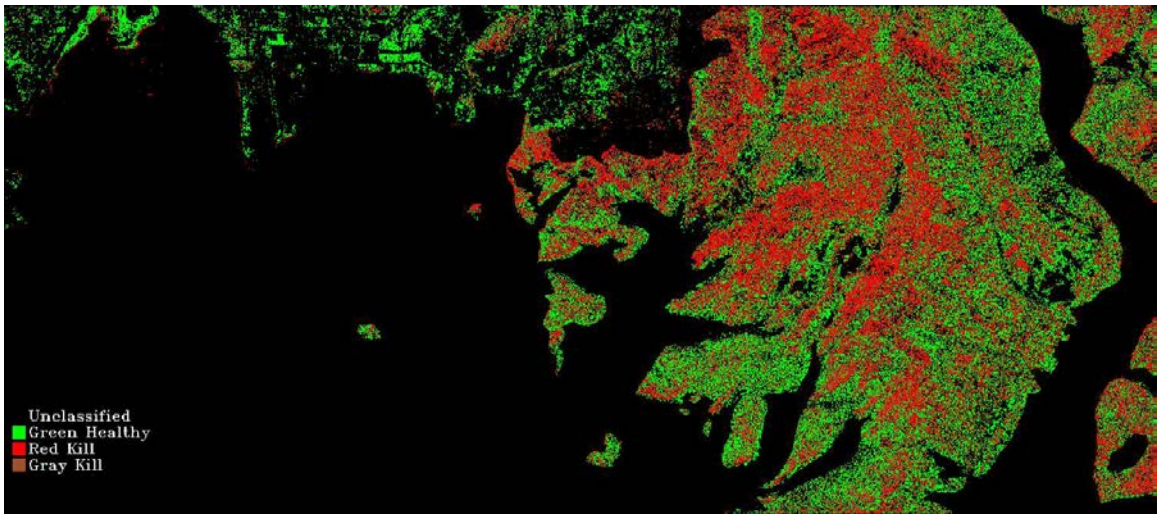

Figure 38. MTMF ratio classification map from July 2009 QuickBird data created by matching regions of interest to image pixel spectra. Image size is 5.952 km by 2.62 km.

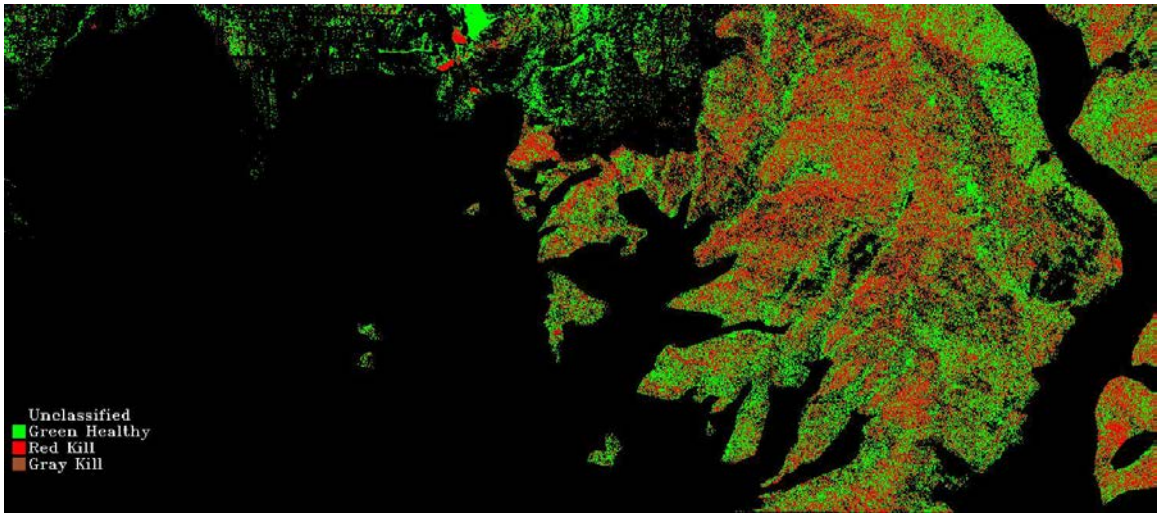

Figure 39. MTMF ratio classification map from June 2011 IKONOS data created by matching regions of interest to image pixel spectra. Image size is 5.952 km by 2.62 km.

In these images it is clear that much more of the forest was classified green healthy throughout the time series. Looking at these classifications, the progression from green, to red, to brown is easier to see. There are, however, some ambiguities, particularly in an apparent progression from grey kill to red kill between 2006 and 2007, then back to red kill in 2009. Unlike the results shown in Figure 33, much of the forest

was mapped as healthy using ROIs for classification. Over time, however, the forest does appear to be dying. Comparing the results from 2009 to 2011 the progression from red kill to gray kill is evident, with much more brown classified in the 2011 image. This should be the case, since it is known that pine beetles kill trees in one year (Wulder et al., 2006).

Classification maps were also created using the ROI spectra for the 2011 AVIRIS data (Figure 40). Again, the results from the two classification maps of 2011 should have shown similar results because they were captured in the same year. Comparing the two images in Figure 39 (2011 IKONOS) and Figure 40 (2011 AVIRIS) showed that this generally was the case, though the AVIRIS data show more gray kill than the IKONOS data. This may be partially explained by mapping of other dry vegetation in the AVIRIS data resulting from the fact that IKONOS data were acquired during June 2011 and the AVIRIS data during August 2011 near the end of the summer season.

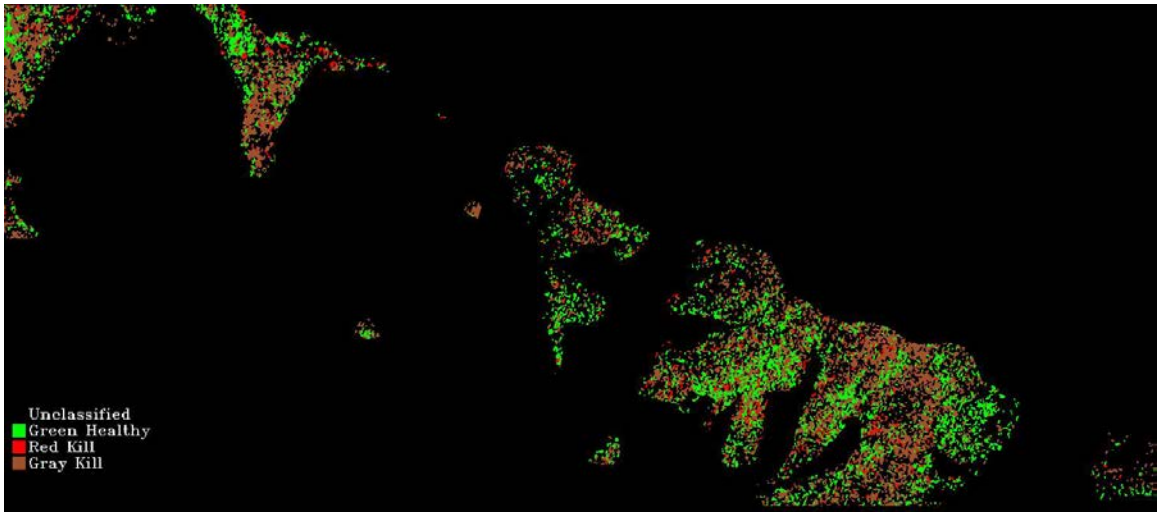

Figure 40. MTMF ratio classification map created by matching ROIs to image pixel spectra from August 2011 AVIRIS. Image size is 5.952 km by 2.62 km.

Visually comparing the results from both classification techniques, change over time is evident, and the data successfully map the progression of tree decay. The classified images mapped from the spectral library show much more red and gray beetle kill than the ROI classified images, but both techniques do show progression from healthy, to unhealthy, to dead. Visual comparison, however, only allow for superficial

comparison. Additional numerical comparisons were attempted to further judge the success of the mapping methods over time.

2. Mathematical Comparison of the MTMF Results over Time

Visual comparison of the data was one way to assess the results of the classification techniques over time. To better understand, and judge the success of the results, confusion matrices were created comparing the classified images and individual parameters from these were plotted to determine apparent trends over time.

Confusion matrices are a common way to represent the classification accuracy of remotely sensed data (Congalton, 1991; Richards and Jia, 2005). Confusion matrices display classification information in an easily readable format of columns and rows that express "the number of sample units (i.e., pixels, clusters of pixels, or polygons) assigned to a particular category relative to the actual category as verified on the ground" (Congalton, 1991). In the confusion matrices created for this study the ground truth pixels are presented in the columns and the MTMF data are presented in the rows. The goal in using the confusion matrices in this research was to track changes in specific classification characteristics over time. This required comparison of individual confusion matrix elements across the datasets.

a. Confusion Matrices between Spectral Library Classification Maps

One way to view the results is to look at the accuracy of the different categories in the confusion matrix (Table 2). The number of correctly classified pixels for each endmember is shown along the main diagonal (highlighted in yellow). Table 2 shows that the AVIRIS spectral library classified image classified 12,200 pixels as green healthy, and the QuickBird spectral library classified image classified 7,543 pixels as green healthy. Between the two years however only 2,515 pixels matched. Based on the knowledge that green healthy trees are declining in the area this number should drop as the years progress.

Class	AVIRIS Green Healthy	AVIRIS Red Kill	AVIRIS Gray Kill	Total
QuickBird Green Healthy	2515	304	4724	7543
QuickBird Red Kill	7857	915	15263	24035
QuickBird Gray Kill	1828	606	5673	8107
Total	12200	1825	25660	39685

Table 2. Confusion matrix of the AVIRIS spectral library classified image and September 2006 QuickBird spectral library classified image comparing classified pixels. The overall accuracy was 22.94 percent with a Kappa coefficient of 0.0141.

Another way to assess the accuracy of the confusion matrix is to look at the Overall Accuracy and the Kappa coefficient. "It is reasonable to expect some degree of agreement will occur by chance alone," and should be removed from consideration (Monserud and Leemans, 1991). The overall accuracy is computed by dividing the total number of correct pixels by the total number of pixels in the error matrix (Congalton, 19991). The Kappa coefficient helps measure how much agreement occurred between each the images being compared, it is equal to one for two maps with perfect agreement and close to zero when the maps agree approximately as much as would be expected due to chance (Monserud & Leemans, 1991). The overall accuracy between the September 2006 classified image and the AVIRIS classified image was 22.94 percent and the Kappa coefficient was 0.0141, suggesting that there was very little agreement between the 2006 QuickBird image and the 2011 AVIRIS image. If the classification results are accurate, the Kappa coefficient should approach one as the years progress between the classification maps.

Errors of omission and commission are also ways to interpret the accuracy of the confusion matrix. Dividing the number of correctly identified pixels in a class by

the number of pixels in the same class "as derived from the reference data," gives errors of omission (Congalton, 1991). Higher omission error represents less accurate classification. Omission error is also called producer's accuracy. Producer's accuracy is a measure of "how well a certain area can be classified," based on the "probability of a reference pixel being correctly classified" (Congalton, 1991). The producer's accuracy of Table 2 for green healthy trees was 20.61 percent, and the omission error was 79.39 percent. Out of a possible 12,200 pixels classified as green healthy, only 2,515 pixels matched between the 2006 QuickBird data and the 2011 AVIRIS data; 9,685 pixels were classified as red or gray kill in the comparison between the 2006 QuickBird data and the 2011 AVIRIS data.

Commission error is determined by dividing the number of correctly classified pixels by the total number of pixels in each class (Congalton, 1991). Errors of commission are also called user's accuracy. User's accuracy represents the probability that a classified pixel "represents that category on the ground" (Congalton, 1991). The user's accuracy of green healthy trees in Table 2 was 33.34 percent, and the commission error was 66.66 percent.

The producer's and user's accuracy for green healthy trees in Table 2 indicate that there were a fair number of matches between the 2006 QuickBird map and the 2011 AVIRIS map. But since it is known from the visual interpretation of the classification images that there was significant change between the two years (the number of green healthy trees has declined since 2006), these results are as expected.

The confusion matrix comparing the August 2007 IKONOS spectral library classified image and the AVIRIS spectral library classified image (Table 3) showed a sharp decline in the number of correctly classified green healthy pixels and large increase in gray kill classified pixels. The overall accuracy of the comparison between the two maps was 29.1 percent with a Kappa coefficient of 0.0179. The producer's accuracy for green healthy declined to 3.61 percent with only 533 pixels out of a possible 14,745 matching for that class. While the number of gray kill pixels correctly classified increased, the producer's accuracy was low but not alarmingly so at 39.58 percent.

Class	AVIRIS Green Healthy	AVIRIS Red Kill	AVIRIS Gray Kill	Total
IKONOS Green Healthy	533	67	935	1535
IKONOS Red Kill	9668	1108	17987	28763
IKONOS Gray Kill	4544	998	12394	17936
Total	14745	2173	31316	48234

Table 3. Confusion matrix of AVIRIS spectral library classified image and August 2007 IKONOS spectral library classified image comparing classified pixels. The overall accuracy was 29.1 percent with a Kappa coefficient of 0.0179.

Table 4 shows the confusion matrix between the July 2009 QuickBird spectral library classified image and the 2011 AVIRIS spectral library classified image. Notice that the number of pixels classified as green healthy has increased, leading to more pixels matching between the AVIRIS and QuickBird maps. This was likely due to above average precipitation for the area over the prior two years, leading to healthier vegetation (particularly grass) in the surrounding areas. The overall accuracy of the confusion matrix in Table 4 was 36.8 percent, with a Kappa coefficient of 0.0682. Producer's accuracies also dropped for both red and gray kill between 2009 and 2007. A number that was shockingly low in this confusion matrix was the user's accuracy for red kill trees, at 4.64 percent. Suggesting that there was a little more than four and a half percent chance that red kill classified pixels on the 2009 QuickBird classification map were actually that class on the ground.

Class	AVIRIS Green Healthy	AVIRIS Red Kill	AVIRIS Gray Kill	Total
QuickBird Green Healthy	4560	466	7037	12063
QuickBird Red Kill	4609	652	8805	14066
QuickBird Gray Kill	2760	714	8989	12463
Total	11929	1832	24831	38592

Table 4. Confusion matrix of AVIRIS spectral library classified image and July 2009 QuickBird spectral library classified image comparing classified pixels. The overall accuracy was 36.8 percent with a Kappa coefficient of 0.0682.

The last confusion matrix comparing spectral library classification maps was between the June 2011 IKONOS map and the 2011 AVIRIS map (Table 5). The number of matched green healthy pixels decreased from 2009, going from 4,560 to 1,968, and the number of matched gray kill classified pixels has increased, going from 8,989 to 10,588.

Class	AVIRIS Green Healthy	AVIRIS Red Kill	AVIRIS Gray Kill	Total
IKONOS Green Healthy	1968	218	3783	5969
IKONOS Red Kill	7516	973	13683	22172
IKONOS Gray Kill	4471	576	10588	15635
Total	13955	1767	28054	43776

Table 5. Confusion matrix of AVIRIS spectral library classified image and June 2011 IKONOS spectral library classified image comparing classified pixels. The overall accuracy was 30.91 percent with a Kappa coefficient of 0.0230.

The results from this confusion matrix show that gray kill classified pixels did increase from 2006, but not as much as expected. The overall accuracy was 30.91 percent with a Kappa coefficient of 0.0230. The user's accuracy for gray kill was fairly high at 67.72 percent, suggesting that almost 68 percent of the time a pixel classified as gray kill will actually represent that feature on the ground.

Figures 41, 42, and 43 show plots of the number of matched pixels between the AVIRIS spectral library classified image and the four multispectral spectral library classified images. Notice that in 2009 the number of matched green healthy pixels is much higher than any of the other years (Figure 41). While the number of green healthy classified pixels that matched between the data sets fluctuates from 2006 to 2011, the overall number of matched pixels for the class went down in that time period from 2,515 in 2006 to 1,968 in 2011. Based on the visual interpretation of the classification images and the known beetle kill cycle, this was the expected result; however, the total was expected to be much lower in 2011 than in 2006.

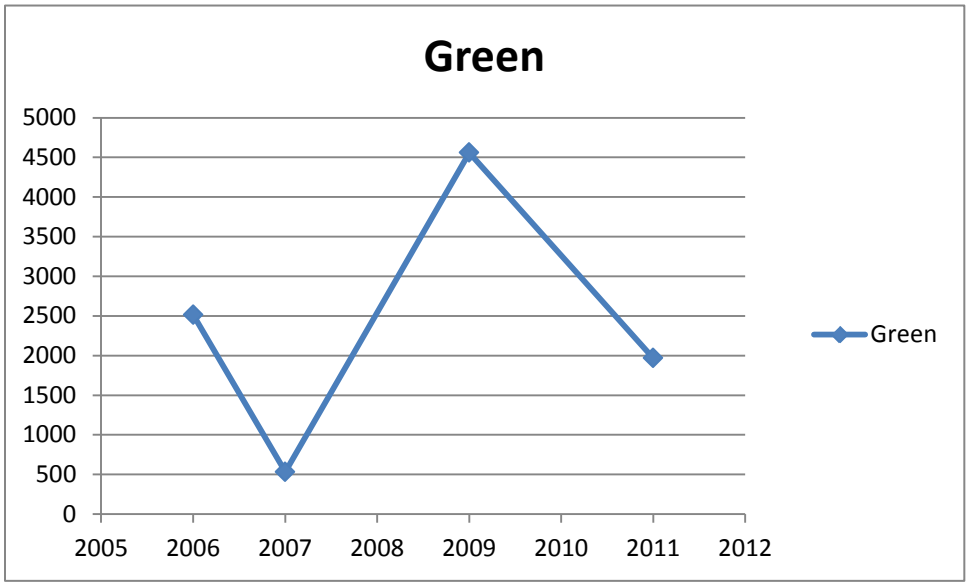

Figure 41. Plot showing the number of green healthy classified pixels matched between the AVIRIS spectral library classification map from 2011 and the classification maps from September 2006, August 2007, July 2009 and June 2011.

Figure 42 shows the plot of matched red pixels between the AVIRIS and spectral library classified image and the four multispectral spectral library classified images. Again, based on the image interpretation and know kill cycle, the number of matched red kill classified pixels should have increased every year from 2006 to 2011; however, because of the 2009 data, which showed much more green healthy growth due to above average rainfall (and insufficiently masked green grass pixels), that number decreased. Additionally, because of the speed with which the trees die and transition from red to gray, the number of red kill classified pixels should remain fairly uniform throughout the years. Overall the number of red kill classified pixels did increase from 2006 to 2011, going from 915 in 2006 to 973 in 2011. A much bigger increase in this classification was expected, but the results did increase over time.

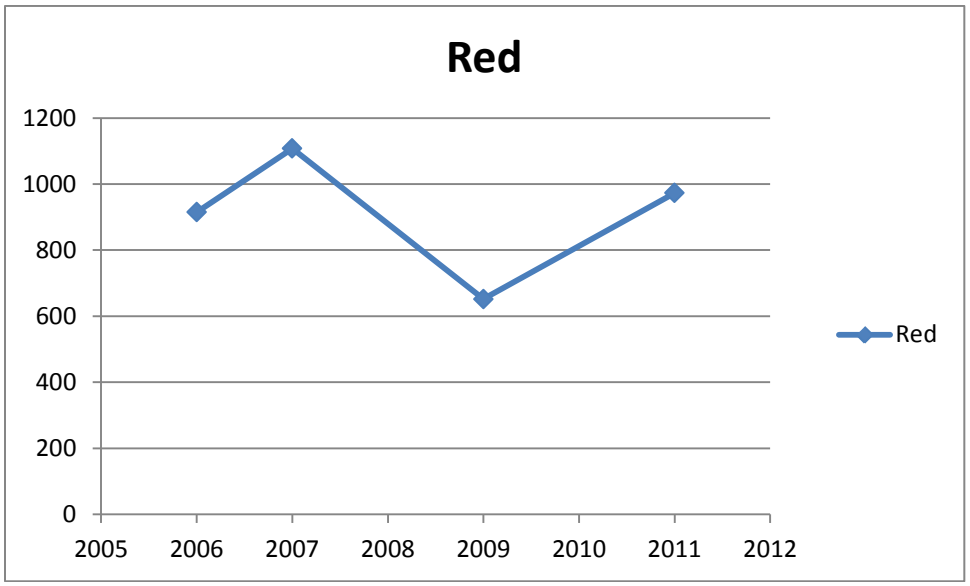

Figure 42. Plot showing the number of red kill classified pixels matched between the AVIRIS spectral library classification map from 2011 and the classification maps from September 2006, August 2007, July 2009 and June 2011.

Figure 43 shows the plot of matched gray kill pixels from the AVIRIS spectral library classified image and the four multispectral spectral library classified images. The plot shows an increase in gray kill from 2006 to 2011, this was the expected result based on visual inspection of the classified images and the known kill cycle. The

number of gray kill classified pixels that matched between the AVIRIS classified image and the multispectral classified images went from 5,673 in 2006 to 10,588.

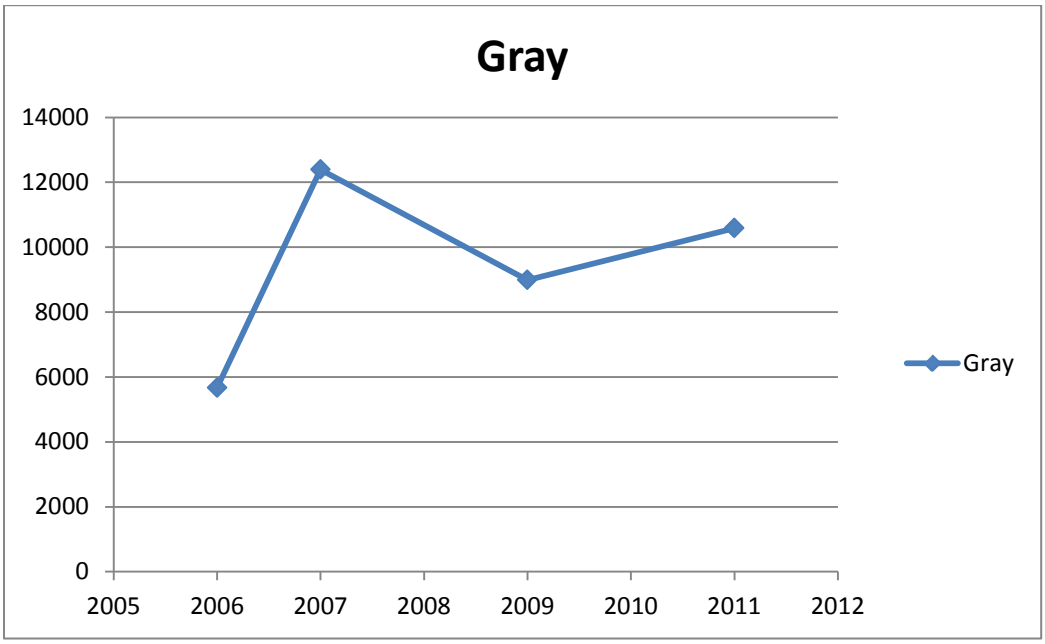

Figure 43. Plot showing the number of gray kill classified pixels matched between the AVIRIS spectral library classification map from 2011 and the classification maps from September 2006, August 2007, July 2009 and June 2011.

b. Confusion Matrices between Regions of Interest Classification Maps

The results from comparing the ROI classification maps were much different than the comparisons between the spectral library classification maps; however, this was expected based on the visual comparisons of the classification results. Table 6 shows the confusion matrix between the September 2006 ROI classification map and the 2011 AVIRIS classification map.

Class	AVIRIS Green Healthy	AVIRIS Red Kill	AVIRIS Gray Kill	Total
QuickBird Green Healthy	7367	5403	4106	16876
QuickBird Red Kill	2781	4528	3197	10506
QuickBird Gray Kill	1075	4108	3113	8296
Total	11223	14039	10416	35678

Table 6. Confusion matrix of AVIRIS regions of interest classified image and September 2006 QuickBird regions of interest classified image comparing classified pixels. The overall accuracy was 42.1 percent with a Kappa coefficient of 0.1320.

Notice the number of green healthy classified pixels is significantly higher than either the red or gray kill classes. This was expected based on the knowledge that there were more green healthy trees in 2006 than red or gray kill trees. The producer's accuracy for green healthy trees was 65.64 percent, which suggested a relatively high match between the AVIRIS and QuickBird region of interest. There were fewer matches for gray kill trees than red kill trees, which was expected based on what is known about mountain pine beetle life cycles. The overall accuracy for the confusion matrix was 42.1 percent while the Kappa coefficient was 0.1320.

Table 7 shows the confusion matrix between the 2007 IKONOS and 2011 AVIRIS classification maps created from comparing regions of interest to image pixel spectra. The results from this comparison show a decrease in both green healthy and gray kill, but an increase in red kill correctly classified pixels. The results in Table 6 show the progression of mountain pine beetle over the course of one year. In September 2006 there were more green trees and fewer red trees, one year later the confusion matrix shows that green healthy trees have decreased and red kill trees have increased. The user's accuracy for all three classes were mid-range, from 36.05 percent for gray kill

classified pixels, to 44.66 percent for red kill classified pixels, to 41.35 percent for green healthy classified pixels, while the producer's accuracies remained fairly close to the previous year's data.

Class	AVIRIS Green Healthy	AVIRIS Red Kill	AVIRIS Gray Kill	Total
IKONOS Green Healthy	6142	4875	3835	14582
IKONOS Red Kill	2947	5524	3897	12368
IKONOS Gray Kill	1424	3868	2983	8275
Total	10513	14267	10715	35495

Table 7. Confusion matrix of AVIRIS regions of interest classified image and August 2007 IKONOS regions of interest classified image comparing classified pixels. The overall accuracy was 41.27 percent with a Kappa coefficient of 0.1177.

The confusion matrix between the July 2009 and AVIRIS 2011 classification maps created from comparing regions of interest to image pixel spectra (Table 8) shows what was expected, a decrease in green healthy trees and an increase in gray kill trees. The user's and producer's accuracies for all three classes held steady showing similar results between the 2009 data and the 2007 data.

Class	AVIRIS Green Healthy	AVIRIS Red Kill	AVIRIS Gray Kill	Total
QuickBird Green Healthy	5301	3641	2916	11858
QuickBird Red Kill	1371	4615	3484	9470
QuickBird Gray Kill	2442	4120	3067	9629
Total	9114	12376	9467	30957

Table 8. Confusion matrix of AVIRIS regions of interest classified image and July 2009 QuickBird regions of interest classified image comparing classified pixels. The overall accuracy of was 41.94 percent with a Kappa coefficient of 0.1332.

The final confusion matrix comparing the regions of interest classification maps was between the June 2011 IKONOS and AVIRIS 2011 data. Table 9 shows decreasing green healthy and gray kill trees with increasing red kill trees. Producer's and user's accuracies were in line with what was observed in all the previous year's data, suggesting that the classification results were consistent.

Class	AVIRIS Green Healthy	AVIRIS Red Kill	AVIRIS Gray Kill	Total
IKONOS Green Healthy	5204	4823	3644	13671
IKONOS Red Kill	2022	4772	3481	10275
IKONOS Gray Kill	1583	3182	2641	7406
Total	8809	12777	9766	31352

Table 9. Confusion matrix of AVIRIS regions of interest classified image and June 2011 IKONOS regions of interest classified image comparing classified pixels. The overall accuracy was 40.24 percent with a Kappa coefficient of 0.1086.

Figures 44, 45, and 46 show the plots for the number of matched pixels between the AVIRIS regions of interest classified image and the four multispectral regions of interest classified images. Figure 45 shows the number of matched pixels classified as green healthy. The number of green healthy classified pixels decreased from 2006 to 2011, going from 7,367 to 5,204 over that period.

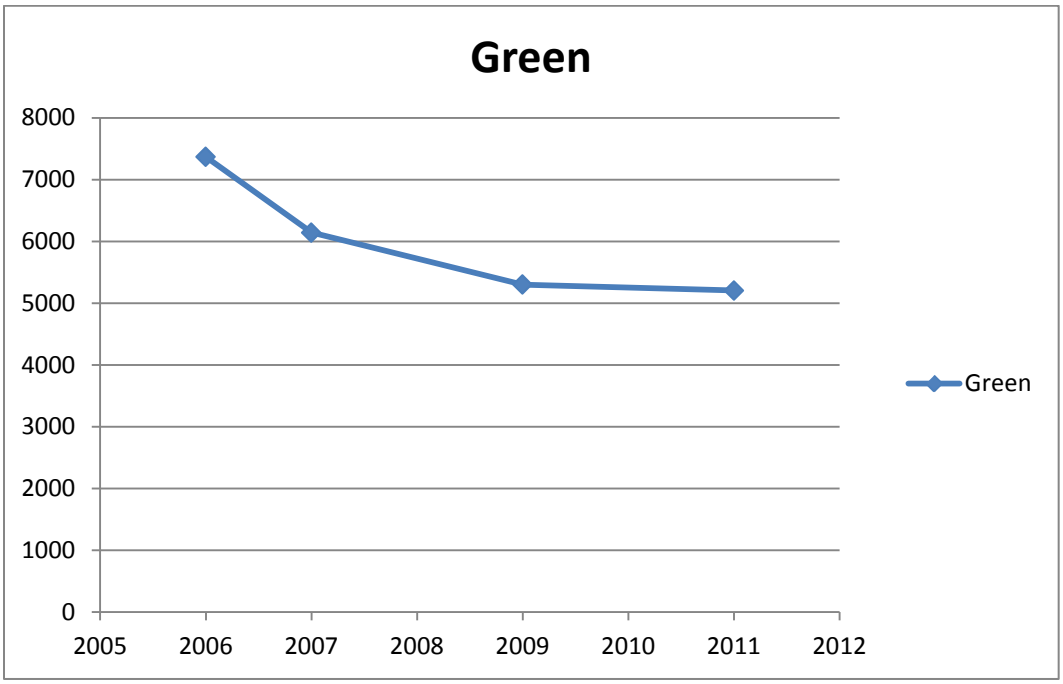

Figure 44. Plot showing the number of green healthy classified pixels matched between the AVIRIS regions of interest classification map from 2011 and the classification maps from September 2006, August 2007, July 2009 and June 2011.

Figure 45 shows the number of matched red kill classified pixels between the AVIRIS regions of interest classified image and the four multispectral classified images. The plot has a similar shape to the other red kill classified image, showing an overall increase in red kill classified trees, but not again not as much as was expected.

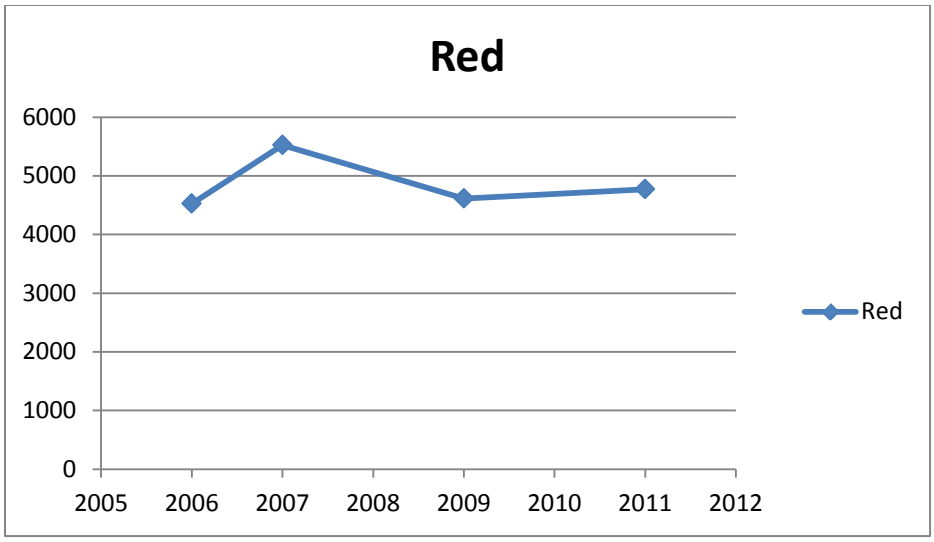

Figure 45. Plot showing the number of red kill classified pixels matched between the AVIRIS regions of interest classification map from 2011 and the classification maps from September 2006, August 2007, July 2009 and June 2011.

Figure 46 shows the number of matched gray kill classified pixels between the AVIRIS regions of interest classified image and the four multispectral classified images. This plot looked nothing like expected, showing a sharp drop off in the number of matched gray kill classified pixels between the AVIRIS and multispectral regions of interest classification maps.

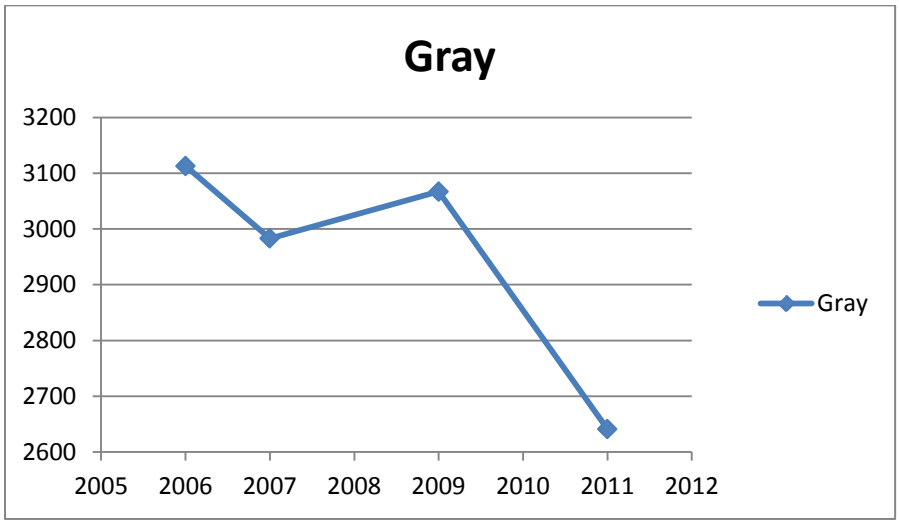

Figure 46. Plot showing the number of gray kill classified pixels matched between the AVIRIS regions of interest classification map from 2011 and the classification maps from September 2006, August 2007, July 2009 and June 2011.

Figures 47, 48, and 49 show the number of total classified pixels from the classification maps created from the spectral library. These plots were not significantly different from the plots showing matched pixels between the HSI and the MSI datasets.

Figure 47 shows that there were fewer total classified green pixels in 2007 than in 2006; however the total increased in 2009 before ultimately dropping in 2011 to below 2006 levels. The increase in green healthy classified pixels in 2009 can be attributed to the wetness of the year. While the decrease in classified pixels is not large, going from 44,638 in 2006 to 41,649 in 2011, the downward trend was what was expected based on the visual classification comparisons and known beetle life cycle.

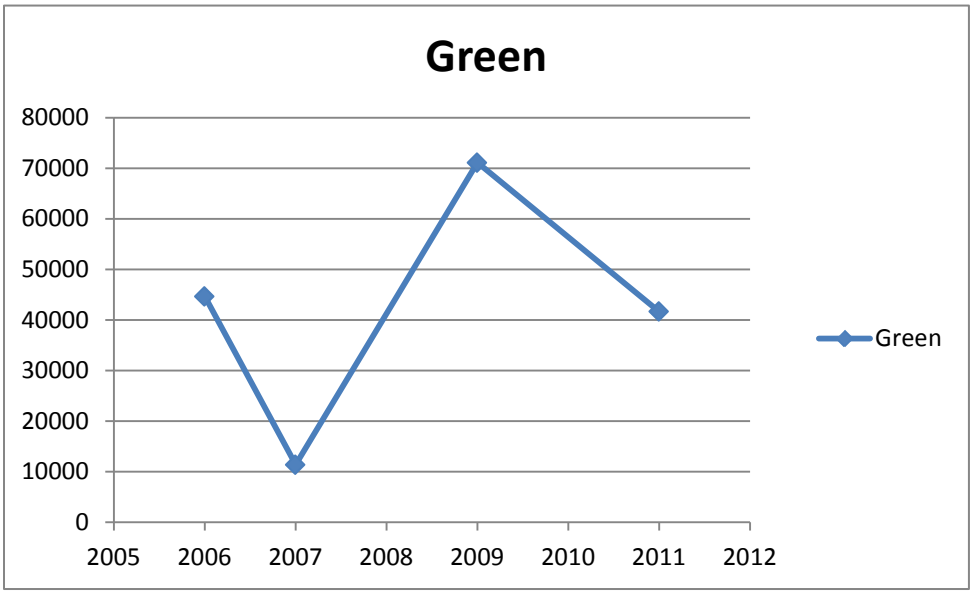

Figure 47. Plot showing the total number of green healthy classified pixels from the spectral library classification method from September 2006, August 2007, July 2009 and June 2011.

Figure 48 shows the total red kill classified pixels from the spectral library classification map. The plot indicates that the number of red kill classified pixels decreased in 2009, which is consistent with what is shown in the classification maps and confusion matrices. As noted previously, the shape of the plot for red kill trees should remain fairly uniform due to the transition speed from red kill to gray kill.

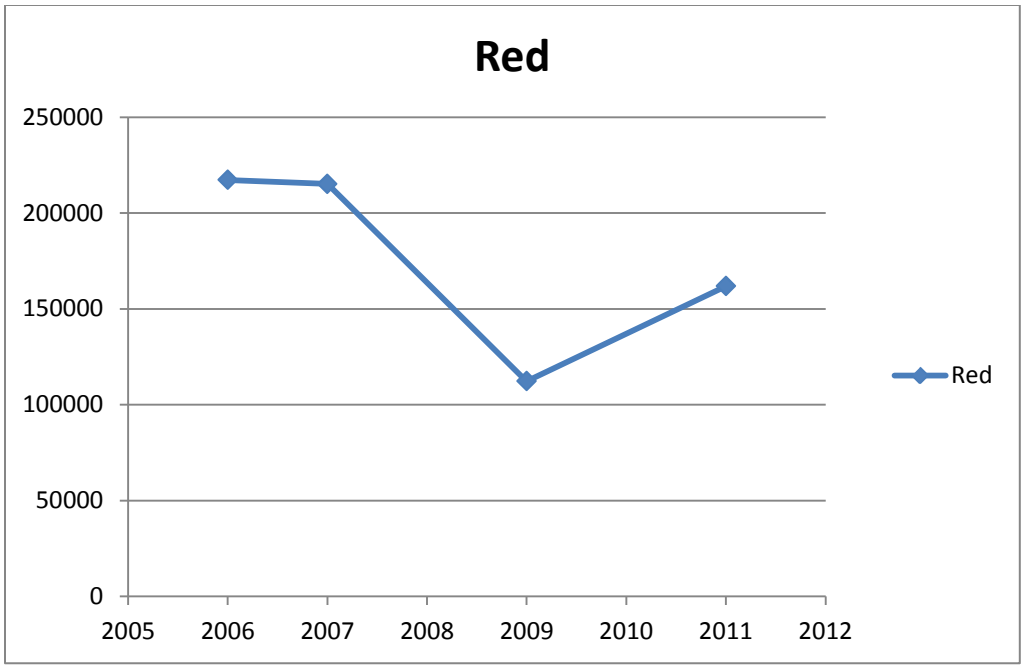

Figure 48. Plot showing the total number of red kill classified pixels from the spectral library classification method from September 2006, August 2007, July 2009 and June 2011.

The total number of gray kill classified pixels did show a large increase from 2006 to 2011, as was expected based on the known beetle life cycle and associated forest decline. Figure 49 shows that the increase in total pixels classified as gray kill was significant. Progressing from 2006 to 2011 the number of gray kill classified went from 54,877 to 145,255.

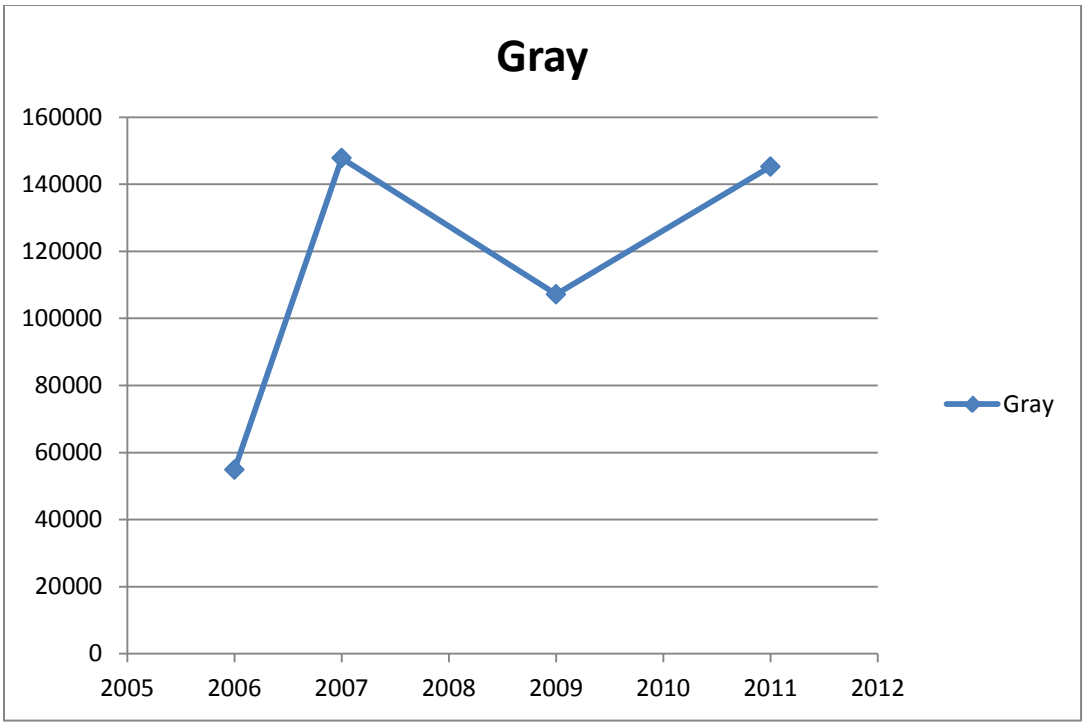

Figure 49. Plot showing the total number of gray kill classified pixels from the spectral library classification method from September 2006, August 2007, July 2009 and June 2011.

Figures 50, 51, and 52 show the number of total classified pixels from the classification maps created from the three regions of interest. It was clear after examining these plots that the trends appear anomalous.

Figure 50 shows that the number of green healthy classified pixels decreased in 2009 and then increased in 2011. The number of green classified pixels was expected to decrease from 2006 to 2011, but based on the spectral library classified images and the results seen, the number of green healthy classified pixels was expected to increase in 2009 and decrease again in 2011.

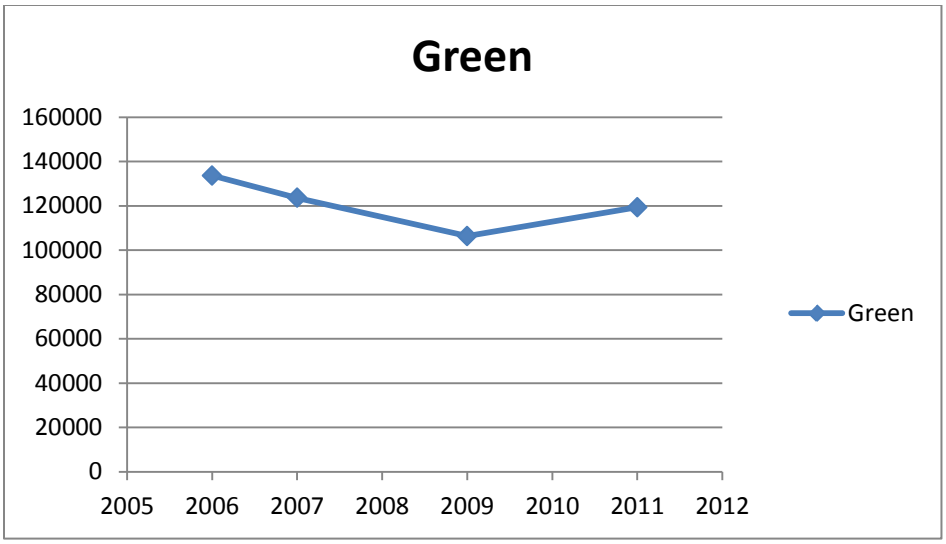

Figure 50. Plot showing the total number of green healthy classified pixels from the regions of interest classification method from September 2006, August 2007, July 2009 and June 2011.

Figure 51 shows that the number of red kill classified pixels remained fairly level from 2006 to 2011. The trend seen in the red kill trees is again what was expected. The results for red classified pixels should be level throughout the years because of the fast transition from red kill to gray kill.

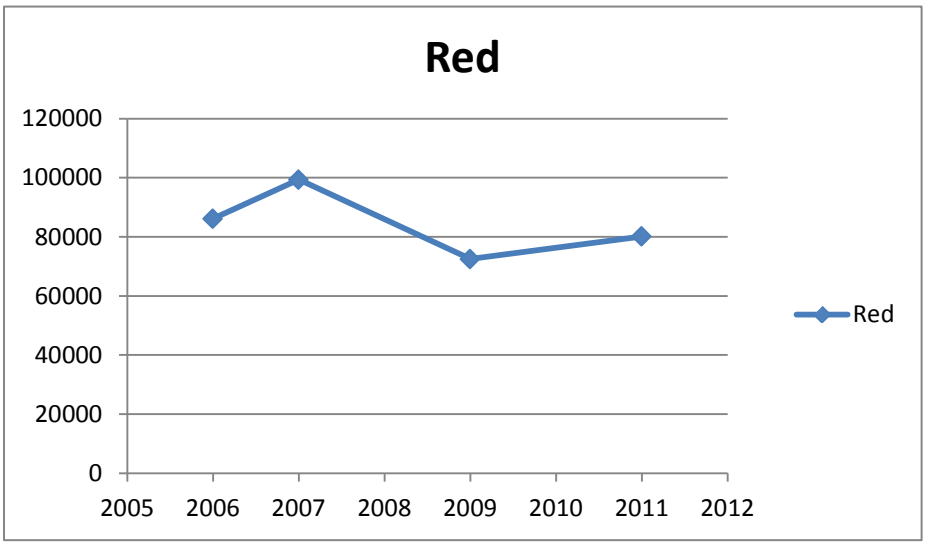

Figure 51. Plot showing the total number of red kill classified pixels from the regions of interest classification method from September 2006, August 2007, July 2009 and June 2011.

Finally, Figure 52 shows a decline in the total number of gray kill classified pixels. This was unexpected, based on the results from the spectral library classified images and what is known about the forest.

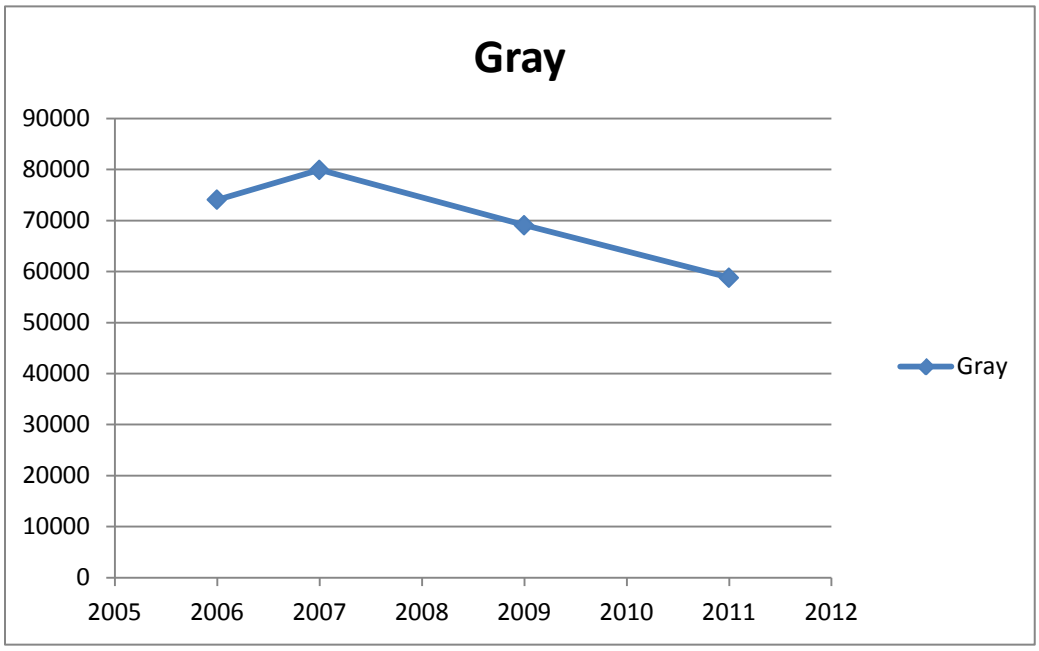

Figure 52. Plot showing the total number of gray kill classified pixels from the regions of interest classification method from September 2006, August 2007, July 2009 and June 2011.

Overall the classification maps produced from regions of interest did not seem to show the same quality of results as those from the library spectra. One reason could be the way the confusion matrices were created. Using the HSI classification map as a baseline to compare the results from the MSI classification maps might have caused those problems. The ROIs were selected from the AVIRIS data, which had 8.9 meter pixels, larger than the 4 meter pixels of the multispectral data. The ROIs were then overlaid on the MSI imagery to create the classification maps; there may have been some ambiguity between the spectral signatures of the AVIRIS pixels and the spectral signatures of the MSI pixels. This seems likely, given the unexpected results from the ROI produced classification maps.

c. Error Sources

There are a number of error sources inherent in the analysis of this time series of multispectral data, starting with the difference between IKONOS and QuickBird multispectral data. Because the IKONOS data had larger pixels the QuickBird data were spatially resized, which may have changed the reflectance characteristics for this data (though nearest neighbor resampling was used to try to minimize this effect). Similarly, the difference in viewing geometry between IKONOS and QuickBird may have also contributed to the inconsistent results. All data need to be radiometrically corrected, and atmospherically corrected to examine spectral characteristics of a scene. To radiometrically calibrate the IKONOS and QuickBird data the processing methods were different, using different factors to compute the radiance values. This processing may have caused inconsistencies between the radiance data, as well as the atmospherically corrected results. Comparing the AVIRIS, IKONOS, and QuickBird data also may have introduced errors. The AVIRIS pixels were more than twice the size of the IKONOS and down sampled QuickBird pixels. Because the pixels from the AVIRIS data were so much larger, this may have led to inconsistencies comparing to the MSI data.

Errors were also potentially caused by the time of year each image was collected. While all the data were captured during the summer, the spectral response can change significantly from month to month. Because these data were not collected during the same month for each year, reflectance values had potential for inconsistency. For example, data from June, a colder month with some possible snow cover, would likely be spectrally different from data collected during July and August, warmer months with variable rainfall, and September, another cold month which is also near the beginning of autumn; all because of changes in vegetation morphology and growth or drying stage. Additionally as the months progressed, illumination of the site changed. Had the data been collected during the same month, results probably would have been different. Using data collected during the same month for each year also would have limited the variability of the spectral response of the features studied. The lodgepole pine trees examined for this study were rapidly changing. Changes occur from month to month, and

due to the variability of the time of year the data were collected, changes in the reflectance characteristics may have been dramatic.

Additional errors may have been caused by the short time span of the data. With only four years of MSI data and only one year of coincident HSI data, it was difficult to gauge the effect of mountain pine beetle. The 2009 MSI collect had a large effect on data trends, significantly altering the results of the study.

Finally, there may have been classification errors throughout. Because the MSI data only had four bands, the degree of match between the spectral library and the spectra from those data was reduced relative to what could be achieved with hyperspectral data. Most of the change in vegetation is seen at the chlorophyll absorption band; however, due to the limited spectral resolution of the MSI data these changes are not as apparent. This may have caused many pixels to go unclassified, thus leading to the poorer than hoped for results.

All of these sources of error combined made this a difficult study and minimization of some of these (not possible within the scope of this study) would probably have dramatically changed the results of this time series analysis.

THIS PAGE INTENTIONALLY LEFT BLANK

V. CONCLUSIONS

The goal of this study was to map the decay of lodgepole pine trees due to mountain pine beetle infestation near Grand Lake, Colorado. Multispectral data spanning a five-year period from 2006 to 2011 were used to assess the progression from live, green trees to dead, gray-brown trees. IKONOS data from 2011 were corrected to reflectance and validated against an AVIRIS hyperspectral dataset, also collected during 2011. These data were used along with additional reflectance-corrected multispectral datasets (IKONOS from 2007 and QuickBird from 2006 and 2009) to create vegetation classification maps using both library spectra and regions of interest. Visual assessment of the image time series and classification results indicated a general progression from the live trees to the dead trees over the five-year period. Problems with data normalization over the time period in question impacted classification efforts, however, and thus lead to some ambiguous results. These observations were also confirmed by quantitative comparison of the classification images. Though not as successful as originally hoped, this research demonstrated the potential for mapping the progression of mountain pine beetle and decay of lodgepole pine trees over time using spectral remote sensing.

With better ground truth data for all the years corresponding to the multispectral data, more accurate classification of the forest could have been possible. Additionally, with matching hyperspectral and multispectral datasets for all the years, spectral signatures would likely have matched better between the images, allowing for more accurate classification. The main problem encountered in this study was the lack of cohesion between the multispectral data sets. The reflectance values were much different between each of the sensors (IKONOS, QuickBird), causing quite a bit of confusion in the classifications. It is also important to note that only five years of data were used for this study. With such a small sample, and particularly with the already advanced stage of the infestation, it was difficult to accurately map the progression of mountain pine beetle damage over time. When such a small sample size is used, one year’s data can significantly skew the final results. In this case, data from 2009, an anomalously wet

year, proved to have a very large effect on classification comparisons. With data from every year of the last decade or longer, the classifications and subsequent comparisons would likely have shown the progression of mountain pine beetle more convincingly and accurately.

Between the two methods of classification the spectral library classification method seemed to be more accurate. Knowing that the forest has degraded over time, the results from the spectral library classification were more conclusive. The ROI classification method did show change over time of the forest; however, the results did not appear to be as accurate as the spectral library classified images. While the confusion matrices showed greater accuracy between the ROI classified MSI and HSI images, the number of pixels classified as gray kill over time went down, which is inconsistent with what is known of the area.

Plots of both total pixel and matched pixel count illustrated the degradation of the forest over time. Additionally, the visual inspection of the classification maps seems to support these findings and results match the known progression of pine beetle damage from healthy green trees, through the red kill stage, to the gray kill stage over time.

LIST OF REFERENCES

Amman, G. D., McGregor, M. D. & Dolph, R. E., Jr. (2002). *Mountain pine beetle.* Retrieved August 13, 2012, from http://www.barkbeetles.org/mountain/fidl2.htm

Associated Press. (2008). Officials say beetles could effectively wipe out all of Colorado's lodgepoles: Infestation that was first detected in 1996 grew by half-million acres last year. *Summit Daily News,* p. A6.

AU Space Primer. (2002). *Multispectral imagery reference guide*. AU Space Primer.

Blakenship, J. R. (2006). *Assessing the ability of hyperspectral data to detect lyngbya SPP.: A potential biological indicator for presence of metal objects in the littoral environment.* Master's thesis, Naval Postgraduate School.

Bobbe, T. J., Alban, J. A., Ishikawa Jr., P., & Myhre, R. J. (1994). An evaluation of narrow-band multispectral video imagery for monitoring forest health. *Remote Sensing and Ecosystem Management: Proceedings of the Fifth Forest Service Remote Sensing Applications Conference*, Portland, Oregon, *5*(1), 191–197.

Colorado Climate Center Colorado State University. (2012). *Colorado precipitation monitoring.* Retrieved September 14, 2012, from http://ccc.atmos.colostate.edu/CO_precip_status.php

Colorado State Forest Service. (2006). *2005 report on the health of Colorado's forests: Special issue aspen forests*. Fort Collins, CO: Author.

Colorado State Forest Service. (2011). *2011 report on the health of Colorado's forests.* Fort Collins, CO: Author.

Congalton, R. G. (1991). A review of assessing the accuracy of classifications of remotely sensed data. *Remote Sensing of Environment, 37,* 35–46.

Cooley, T., Anderson, G. P., Felde, G. W., Holke, M. L., Ratkowski, A. J., Chetwynd, J. H., et al. (2002). FLAASH, a MODTRAN4-based atmospheric correction algorithm, its application and validation, *3*, 1414–1418.

DeRose, R. J., Long, J. N., & Ramsey, R. D. (2011). Combining dendrochronological data and the disturbance index to assess engelmann spruce mortality caused by a spruce beetle outbreak in Southern Utah, USA. *Remote Sensing of Environment, 115*(9), 2342–2349.

DigitalGlobe. (2012). *QuickBird spacecraft data sheet.* Retrieved August 14, 2012, from http://www.digitalglobe.com/downloads/WorldView1-DS-WV1-Web.pdf

Eismann, M. T. (2012). *Hyperspectral remote sensing*. Bellingham, Washington: SPIE Press.

Fantle, M. (2010). *Passive remote sensing.* Retrieved July 18, 2012, from https://wikispaces.psu.edu/display/RemSens597K/P

Gao, B. C., Davis, C. O., & Goetz, A. F. H. (2006). A review of atmospheric correction techniques for hyperspectral remote sensing of land surfaces and ocean color. *Geoscience and Remote Sensing Symposium.*

GeoEye. (2012). *IKONOS fact sheet.* Retrieved August 14, 2012, from http://www.geoeye.com/CorpSite/products/earth-imagery/geoeye-satellites.aspx#ikonos

Goetz, A. F. H. (2012). Foreword. In P. S. Thenkabail, J. G. Lyon & A. Huete (Eds.), *Hyperspectral remote sensing of vegetation* (1st ed., pp. ix-x). Boca Raton, FL: CRC Press.

Goetz, A. F. H., Vane, G., Solomon, J. E., & Rock, B. N. (1985). Imaging spectrometry for earth remote sensing. *Science, 228*(4704), 1147–1153.

Green, A. A., Berman, M., Switzer, P., & Craig, M. D. (1988). A transformation for ordering multispectral data in terms of image quality with implications for noise removal. *IEEE Transactions on Geoscience and Remote Sensing, 26*(1), 65–74.

Green, R. O., Eastwood, M. L., Sarture, C. M., Chorine, T. G., Aaronson, M., Chippendale, B. J., et al. (1998). Imaging spectroscopy and the airborne Visible/Infrared imaging spectrometer (AVIRIS). *Remote Sensing of Environment, 65*(3), 227–248.

Gustafsson, A. (1993). *Interactive image warping.* Masters thesis, Helsinki University of Technology, Helsinki, Finland.

Hadjimitsis, D. G., Papadavid, G., Agapiou, A., Themistocleous, K., Hadjimitsis, M. G., Retalis, A., et al. (2010). Atmospheric correction for satellite remotely sensed data intended for agricultural applications: Impact on vegetation indices. *Natural Hazards and Earth System Sciences, 10*, 89–95.

Hartman, T. (2008). Deaths of trees ‘catastrophic’. *Rocky Mountain News,*

Jenkins, M., Page, W., Hebertson, E., & Alexander, M. (2012). Fuels and fire behavior in bark beetle attacked forests in western north america and implications for fire management. *Utah State University Digital Commons at USU, 275*, 23–34.

Jensen, J. R. (2005). *Introductory digital image processing* (3rd ed.). Upper Saddle River, NJ: Prentice Hall.

Jet Propulsion Laboratory. (2012). *AVIRIS: Airborne Visible/Infrared imaging spectrometer.* Retrieved August 15, 2012, from http://aviris.jpl.nasa.gov/aviris/index.html

Knipling, E. B. (1970). Physical and physiological basis for the reflectance of visible and near-infrared radiation from vegetation. *Remote Sensing of Environment, 1*(3), 155–159.

Kruse, F. A., & Perry, S. L. (2009). Improving multispectral mapping by spectral modeling with hyperspectral signatures. *Journal of Applied Remote Sensing, 3*(1)

Kumar, A., Lee, S. W., Ehsani, R. J., Albrigo, L. G., Yang, C., & Mangan, R. L. (2012). Citrus greening disease detection using aerial hyperspectral and multispectral imaging techniques. *Journal of Applied Remote Sensing, 6*(1), 1–21.

Leatherman, D. A., Aguayo, I. & Mehall, T. M. (2011). *Mountain pine beetle.* Retrieved July 3, 2012, from http://www.ext.colostate.edu/pubs/insect/05528.html/

Lillesand, T. M., & Kiefer, R. W. (1994). *Remote sensing and image interpretation* (3rd ed.). New York: John Wiley & Sons.

Madrigal, A. (2007). *The natural pine-beetle ecosystem goes off its rails.* Retrieved Ausuts 09, 2012, from http://www.wired.com/wiredscience/2007/11/the-natural-pin/

Matthew, M. W., Adler-Golden, S. M., Berk, A., Felde, G., Anderson, G. P., Gorodetzky, D., et al. (2002). Atmospheric correction of spectral imagery: Evaluation of the FLAASH algorithm with AVIRIS data, *31*. pp. 157–163.

Mattson, B. (2010). *Electromagnetic spectrum.* Retrieved July 18, 2012, from http://imagine.gsfc.nasa.gov/docs/science/know_l1/emspectrum.html

Meddens, A. J. H., Hicke, J. A., & Vierling, L. A. (2011). Evaluating the potential of multispectral imagery to map multiple stages of tree mortality. *Remote Sensing of Environment, 115*, 1632–1642.

Monserud, R. A., & Leemans, R. (1991). Comparing global vegetation maps with the kappa statistic. *Ecological Modeling, 62*, 275–293.

National Park Service. *Rocky mountain national park map.* Retrieved August10, 2012, from http://www.nps.gov/common/commonspot/customcf/apps/maps/showmap.cfm?alphacode=romo&parkname=Rocky%20Mountain

Richards, J. A., & Jia, X. (1999). *Remote sensing digital image analysis* (3rd ed.). Berlin, Germany: Springer.

Roberts, D. A., Yamaguchi, Y., & Lyon, R. (1986). Comparison of various techniques for calibration of AIS data. *Proceedings of the 2nd Airborne Imaging Spectrometer Data Analysis Workshop,* Pasadena, *86*(35), 21–30.

Romme, W. H., Knight, D. H., & Yavitt, J. B. (1986). Mountain pine beetle outbreaks in the rocky mountains: Regulators of primary productivity? *The American Naturalist, 127*(4), 484–494.

Satnews Daily. (2010). *Lockheed martin + GeoEye...eleven image-filled years (imagery).* Retrieved August 15, 2012, from http://www.satnews.com/cgi-bin/story.cgi?number=1485529201

Schowengerdt, R. A. (2007). *Remote sensing: Models and methods for image processing*. Burlington, MA: Academic Press.

Shaw, G. A., & Burke, H. K. (2003). Spectral imaging for remote sensing. *Lincoln Laboratory Journal, 14*, 3–28.

Short, N. M. (2007). *Comparison of hyperspectral to multispectral data.* Retrieved July 21, 2012, from http://www.fas.org/irp/imint/docs/rst/Sect13/Sect13_9.html

Skakun, R. S., Wulder, M. A., & Franklin, S. E. (2003). Sensitivity of thematic mapper enhanced wetness difference index to detect mountain pine beetle red-attack damage. *Remote Sensing of Environment, 86*(4), 433–443.

Smith, G. M., & Milton, E. J. (1999). The use of empirical line method to calibrate remotely sensed data to reflectance. *International Journal of Remote Sensing, 20*(13), 2653–2662.

United States Forest Service. (2007). *NFS acreage by state, congressional district and county.* Retrieved August 8, 2012, from http://www.fs.fed.us/land/staff/lar/2007/TABLE_6.htm

Ustin, S. L., Roberts, D. A., Gamon, J. A., Asner, G. P., & Green, R. O. (2004). Using imaging spectroscopy to study ecosystem processes and properties. *BioScience, 54*(6), 523–534.

White, J. C., Coops, N. C., Hilker, T., Wulder, M. A., & Carroll, A. L. (2007). Detecting mountain pine beetle red attack damage with EO-1 Hyperion moisture indices. *International Journal of Remote Sensing, 28*(10), 2111–2121.

White, J. C., Wulder, M. A., Brooks, D., Reich, R., & Wheate, R. D. (2005). Detection of red attack stage mountain pine beetle infestation with high spatial resolution satellite imagery. *Remote Sensing of Environment, 96*(3–4), 340–351.

Wulder, M. A., White, J. C., Bentz, B., Alvarez, M. F., & Coops, N. C. (2006). Estimating the probability of mountain pine beetle red-attack damage. *Remote Sensing of Environment, 101*(2), 150–166.

THIS PAGE INTENTIONALLY LEFT BLANK

INITIAL DISTRIBUTION LIST

1. Defense Technical Information Center
   Ft. Belvoir, Virginia

2. Dudley Knox Library
   Naval Postgraduate School
   Monterey, California

3. Fred A. Kruse
   Naval Postgraduate School
   Monterey, California